Sliding Mode Extremum Seeking Control for Maximum Power Extraction in Wave Energy Converters

by

Adlin Sharon Vinola Alwyn Ravi Kumar

B.Tech., SRM Institute of Science and Technology, 2018

Thesis Submitted in Partial Fulfillment of the
Requirements for the Degree of
Master of Applied Science

in the
School of Mechatronic Systems Engineering
Faculty of Applied Sciences

SIMON FRASER UNIVERSITY
Fall 2022

Declaration of Committee

Name:	**Adlin Sharon Vinola Alwyn Ravi Kumar**
Degree:	**Master of Applied Science**
Thesis title:	**Sliding Mode Extremum Seeking Control for Maximum Power Extraction in Wave Energy Converters**
Committee:	**Chair:** Ramtin Rakhsha Lecturer, Mechatronic Systems Engineering
	Mehrdad Moallem Supervisor Professor, Mechatronic Systems Engineering
	Helen Bailey Committee Member Lecturer, Mechatronic Systems Engineering
	Jason Wang Examiner Associate Professor, Mechatronic Systems Engineering

Abstract

Renewable energy is a revolution in the field of power generation to ensure environment friendly alternatives to fossil fuels. Wave power is a huge source of renewable energy found in the ocean's waves. In this research, the main objective is to extract maximum wave power from the near-shore waves in multiple degrees-of-freedom (DOF). In order to achieve this goal, a combination of design, control, and energy transfer parameters are considered to extract energy from buoy motions that are applied to a multi DOF robotic wave energy converter (WEC). The specific design of a buoy and dynamic modeling of a 2 DOF WEC are used in a case study as a robotic arm acting in a reverse mode, i.e., conversion of mechanical energy into electric power acting in pitch and heave direction of motion. The power extraction algorithm is controlled by a sliding mode extremum seeking (SM-ES) method that ensures the same phase trajectory in the face of multiple frequency regular wave patterns. Simulation analyses are introduced to exhibit the execution of the power extraction scheme and its productiveness. Furthermore, the performance of the proposed controller is compared with a latching control method. According to the results, the proposed controller offers superior performance in terms of power absorbed.

Keywords: Maximum power transfer, nearshore WEC, adaptive control, sliding mode extremum seeking, time-domain dynamic modeling

Dedication

To my supportive parents Alwyn, Rachel, and my inspiring brother Dr.Alan.

Acknowledgements

This thesis and the research behind it would not have been possible without the exceptional support of my supervisor, Dr.Mehrdad Moallem. His enthusiasm, knowledge and exacting attention to detail have been an inspiration and kept my work on track from my first encounter with the rough drafts to the final draft of this thesis. Dr.Helen Bailey, an expert in Ocean Technology at Simon Fraser University, has also looked over my transcriptions and answered with unfailing patience numerous questions about wave theories and marine technology. I am most thankful for the MITACS Accelerate program alongside the partner organization, Oceanergy Technologies Ltd. that provided financial support for the larger project from which this thesis grew. Finally, I am also grateful for the insightful comments offered by my family, my friends, and my colleagues. The generosity and expertise of one and all have improved this study in innumerable ways.

Table of Contents

List of Tables

List of Figures

Chapter 1

Introduction

1.1 Wave Energy

The energy generated from the motion of waves is called wave energy. Waves are generated depending on the winds; therefore, can vary in size and frequency. Wave energy harvesting is affected by multiple variables, such as the wave height, wave speed, wavelength, and wave period [1]. It can be harnessed in a variety of ways, similar to solar, wind, and geothermal energy. With the advancement of technologies, renewable energy researchers are exploring ways of harnessing more power from waves and the ocean. Although it is emerging as a new potential source for renewable energy generation, with wave energy technology the cost is not cost-effective with other more mature renewable energy sources such as wind and solar energy. One approach that researchers and developers are taking to reduce the cost of wave energy is to actively control wave energy converters (WECs), increasing the average power production dramatically. Most of the proposed control algorithms depend on predictions of the future wave excitation forces and moments, as the optimal control action depends on these future forces.

This thesis details a methodology that uses a model-free approach to control the velocity of the WEC. The methodology is tested on a robotic, 2 degrees-of-freedom (DOF), point absorbing WEC in simulations, using time series data as input to the WEC model. The proposed controller's performance is compared with a latching controller and the results analyzed.

1.2 Research Context

Ocean wave resources are harnessed using a combination of components to produce electricity, collectively forming a WEC device. Currently, there are few WEC implementations in the ocean, but most are not commercially viable compared to other mature renewable resources like wind and solar.

For wave energy to become a cost competitive source of electricity, its levelized cost of electricity (LCOE) must be reduced. LCOE can be reduced in two main ways; the cost of a wave energy converter can be reduced without impacting the power production, or WECs can be designed to produce more power without significantly impacting the cost of the device. In reality, both of these factors need to be addressed to continue to reduce the LCOE.

One current area of research to increase the amount of power produced by a WEC is to actively control it in such a way that average power output can be increased. The power take-off (PTO) system can be configured to vary the amount of force exerted on the WEC and maximize power output. This has been an active area of research, with control algorithms such as wave excitation forces and moments prediction methods [2, 3, 4] of realistic wave models, allowing for more accurate WEC control. For example, the parametric wave prediction model [5], autoregressive (AR) predictive model [6] and recurrent neural network prediction model [7] have been some of the most popular methods. Unfortunately, some of these schemes deploy off-line prediction algorithms, which do not account for real-time uncertain variation. Additionally, the control methods proposed [8] are reliant on the accuracy of the prediction models, which constrains their performance. Moreover, for the WEC to operate effectively, the wave excitation force and moment needs to be predicted several seconds in the future [9]. Therefore, practical applications may be limited if a wave prediction model is necessary for control.

Currently, real-time adaptive control methods have been used in industrial nonlinear applications for tuning variable controller parameters [10, 11, 12, 13]. Extremum seeking (ES) is a trending real-time learning control technique that does not require previous knowledge of the system input–output [14]. Hence, it is a good solution to address min-max optimization problems such as velocity profile regulation [15], variable-gain control [16] and maximum power-point tracking [17]. This work presents a sliding-mode extremum seeking (SM-ES) approach to control the velocity of the WEC.

Also, in comparison to other WEC technologies, the point absorber type is a relatively compact device [18]. Therefore, the cost of the device may be lower in comparison to other types of WEC. However, due to their size, point absorbers can have a very small range of wave frequencies for which the WEC performs at its maximum potential. Additionally, due to other practical factors, such as unpredictability of the ocean wave patterns and non-linear effects, point absorbers are limited in their function to absorb maximum power constantly [19, 20, 21]. Previously, specific float geometries have been implemented depending on the sea state of the desired WEC deployment location [22, 23]. These various approaches also highlight the environmental and ecological effects of wave energy, its conversion technologies, and control strategies. This thesis includes the design of a buoy geometry based on the sea state in the chosen deployment location.

1.2.1 Thesis Objective

In this study, a multi degree-of-freedom serial chain point absorber type of WEC with a sliding mode extremum seeking controller that enables maximum power extraction is proposed. The WEC system proposed also extends conventional point absorber WEC systems [24] such as WaveStar [25, 26] and PowerBuoy [27], since it combines robotic concepts.

The proposed methods are applied to a customized 2 DOF manipulator designed specifically for a near-shore application which is connected rigidly to a specialized buoy designed to capture maximum force from the incident wave. Furthermore, the study includes features in the manipulator to capture wave energy from two wave force components, specifically heave forces and pitch moments. In addition to maximizing power, the proposed extremum seeking controller also maintains a desired velocity function that keeps the WEC absorbing maximum average power at all times. The sliding mode algorithm [28] eliminates the need for predictive models, thereby making the approach model-free. A summary of the general objectives of this research are listed as follows:

- **Robotic Wave energy conversion system:** By incorporating concepts from robotics, power electronics, and control, into the design of wave energy converters, a main thrust of the research is to develop integrated mechanical and control-based feedback systems that can maximize energy extraction under the time-varying wave conditions while meeting other criteria such as dual energy capture (from two force components).

- **Simulation of a Proof-of-concept wave converter device:** A 3-D CAD model is developed with the project as a near-shore wave energy converter. The simulation results will be obtained using the MATLAB-Simulink environment.

1.2.2 Methodology

The initial phase of this thesis was finalizing the near-shore location. Then, the WEC was designed based on the wave parameters of the chosen location and the controller simulated in the MATLAB-Simulink environment. The simulation system would ideally provide a baseline for performance parameters of a scaled-up system under more constrained conditions. Once the location was chosen, a moving body in contact with a fixed structure that absorbs energy from the relative motion of the waves was required. The point-absorber type of wave energy converter was selected. Then, a floating buoy was designed to harness energy with a few modifications to a regular point absorber type WEC. The goal in the design process was to have both less submerged and underwater components of the overall WEC system, reducing the risk of bio-fouling. Further details pertaining to the location selection and buoy design are found in Chapter 4.

The buoy was envisioned to raise and lower a robotic arm located at a near-shore pivot point. Hence, the robot was designed as an open kinematic chain to host the buoy

connected rigidly to it. The robot included a prismatic and a rotary joint for capturing power from both the heaving and pitching mode respectively. When the arm is connected directly to an electromechanical converter along with power electronics and control circuitry, it would enable direct translation of the captured wave energy. Each robot joint is assumed to be connected directly to a generator ensuring direct mechanical translation to electricity, reducing the loss of energy transfer. Robots are well-known for their precise automation in harsh, unpredictable conditions, hence a robot as a WEC was chosen in this thesis. Further details are found in Chapter 4.

In order to enable maximum power absorption, the WEC should also be a good wave generator. To achieve this, a power transfer function was found using the WEC as an open kinematic chain robot model. The system however must adapt automatically to the changes in the wave's unpredictable environment. Therefore, an extremum seeking controller (ESC) was explored. The ESC algorithm would find the desired speed at which maximum average power is absorbed, and the sliding mode would get the desired speed to obtain maximum power transfer. Further details on how the ESC is implemented is described in Chapters 3 and 4.

1.3 Chapter Breakdown

This thesis document is organized as follows.

Chapter 2 begins with the classification of WECs according to the structure and power harnessing orientation. This classification is inherently meaningful because it can be related to the research objective. The second half of Chapter 2 includes the dynamic interaction between the sea state, the buoy and the WEC. The dynamic model is described in the time-domain. An overview of widely used theories of the sea state and dynamics of a WEC is presented. It also discusses the underlying assumptions behind the simulation and common sources of ambiguity.

Chapter 3 discusses well-known theories of linear control for WECs. In later chapters, the performance of the author's control scheme is plotted alongside the performance of another popular scheme. The author's control scheme to ensure maximum power absorption based on controlling the speed of the buoy is introduced in the second half of this chapter. The chapter ends with a literature review on extremum seeking control, a description of the proposed sliding mode extremum seeking controller and a brief explanation of the latching controller used in this thesis.

Chapter 4 focuses on the case study introduced for simulation purposes. The design of the floating buoy to extract maximum power from the incident wave is explored. The next part of the chapter dives into the design and modeling of a 2 DOF open kinematic chain WEC that is connected rigidly to the buoy and based near-shore. The last part of Chapter 4 introduces the two controllers used to study and compare the interaction between the sea

state and the average power absorbed due to the combined effects of the 2 DOF WEC and floating buoy.

Chapter 5 includes an introduction to the WEC simulation software used in this research, called WEC-Sim. The simulation results of the WEC model in WEC-Sim and the MATLAB-Simulink environment are also presented in this chapter. The results are discussed and the controller performances compared.

Chapter 6 summarizes the work in this thesis. Opportunities presented by this research are gathered together as recommendations for further industrial and academic research.

Chapter 2

Wave Energy Converter

WEGEMT (a European association of 40 universities in 17 countries) defines marine technology as "technologies for the safe use, exploitation, protection of, and intervention in, the marine environment" [29]. According to WEGEMT this includes: naval architecture, marine engineering, ship design, ship building, ship operations, hydrodynamics, navigation, sea surface and subsurface support, underwater technology, marine resources (including both renewable and non-renewable marine resources) and many more.

A broad range of technologies that derive energy from the ocean are known as marine renewables. This energy can be harvested from ocean waves, tidal movements, or thermal gradients. Wave energy technologies capture kinetic (motion) energy from the ocean's waves to perform useful functions such as generating electricity. The WEC converts the kinetic and potential energy of a moving ocean wave into mechanical energy or electrical energy.

2.1 Review of Current Wave Energy Converters

Depending on the location of deployment, wave energy converters can produce electricity either near-shore, on-shore or offshore. WEC's can be further classified based on their structural movements as attenuators, point absorbers, surge converters, oscillating water columns(OWC), overtopping devices, and submerged pressure differential devices.

A few examples of wave energy converters previously deployed or currently deployed in the oceans around the world are the OWC by the 150 kW Indian Wave Energy Program [30], surface-following attenuator by Pelamis Wave Power [31], Denmark's overtopping device called Wave Dragon [32] and a WEC with multipoint absorbers called Wave Star [33].

2.1.1 Attenuators

Attenuators are floating devices with multiple segments that function parallel to the wave direction and flex as differing wave heights occur, thereby capturing energy from the relative motion of the segments as the wave passes them. Figure 2.1 shows an attenuator type of WEC called Pelamis.

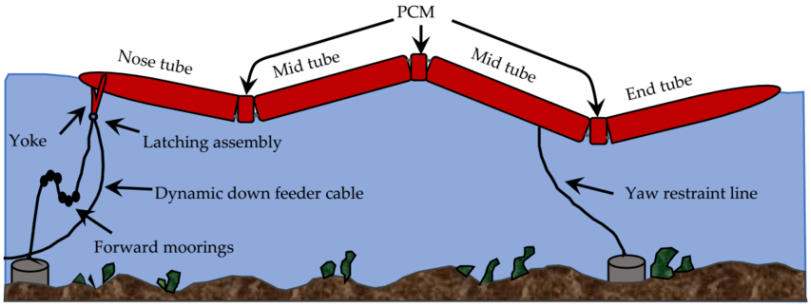

Figure 2.1: Pelamis Attenuator - Wave Energy Harnessing Device [34]

2.1.2 Oscillating wave surge converter

An oscillating wave surge converter typically has a fixed end and a free end. Energy is collected from the relative motion of the body, which is a result of waves moving horizontally (surge) to the fixed end. An example of an oscillating wave surge converter is depicted in Figure 2.2.

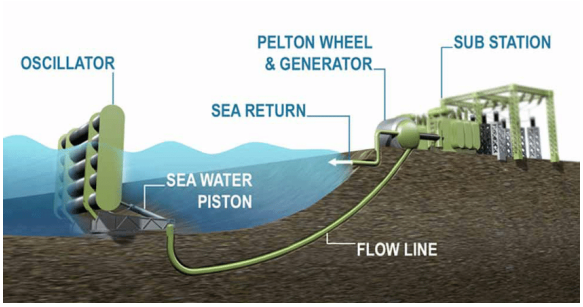

Figure 2.2: Oscillating Wave Surge — Energy Harnessing Device [35]

2.1.3 Oscillation water column

An oscillating water column is partially submerged and hollow as seen in Figure 2.3. The hollow structure allows the water column to rise and fall with respect to the waves, which in turn compresses and decompresses the air column, resulting in an air flow that moves a turbine generating energy.

2.1.4 Overtopping device

In overtopping devices, water is captured as waves break into a reservoir, generating additional energy through waves. Figure 2.4 shows a type of overtopping device with a turbine outlet.

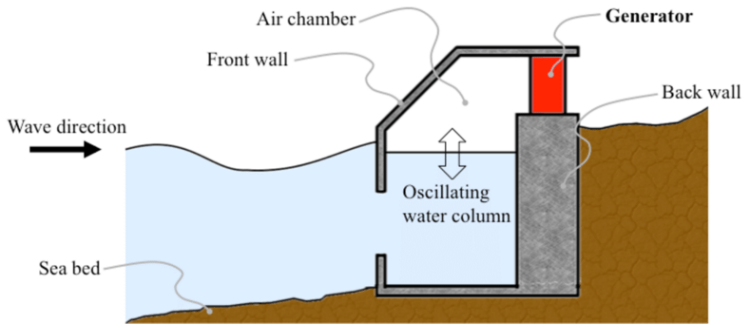

Figure 2.3: Oscillating Water Column - Wave Energy Harnessing Device [36]

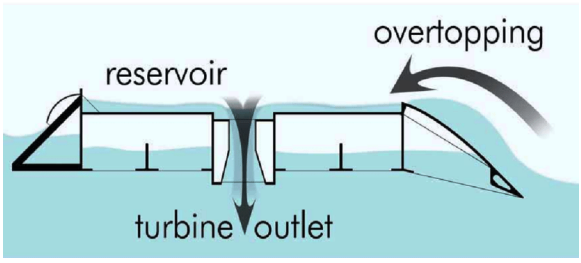

Figure 2.4: Overtopping - Wave Energy Harnessing Device [37]

2.1.5 Submerged pressure differential

As sea level rises and falls above the submerged device, the motion of the waves causes a pressure differential within it. This alternating pressure pumps fluid through a system to generate electricity. Figure 2.5 shows this type of submerged device with a displacer and a reactor.

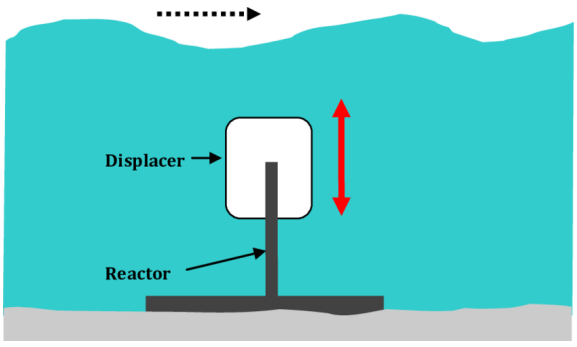

Figure 2.5: Submerged Pressure Differential - Wave Energy Harnessing Device [38]

2.1.6 Point Absorbers

Point absorbers are floating structures that absorb energy from all directions through their movement on the water surface. The point absorber produces electricity by using the motion of the buoyant top relative to the base. In this research, a point absorber type of WEC is chosen due to its ability of harnessing power with fewer points of contacts that are submerged or underwater. As opposed to Figure 2.6 that shows a submerged PTO system, point absorbers can also be designed to have dry PTO systems that can be connected near-shore easily. The dry PTO point absorbers are subject to lower maintenance as they have fewer parts exposed to the ocean water, leading to less bio-fouling and wear-and-tear. The

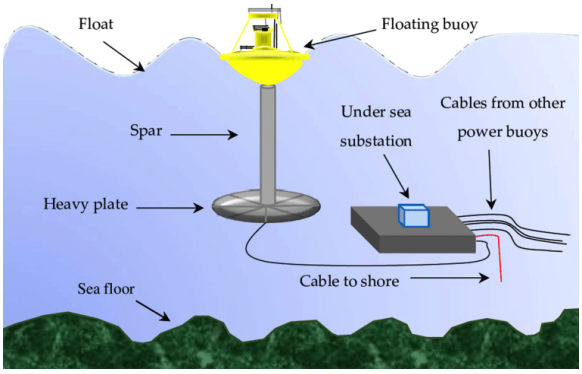

Figure 2.6: Point Absorber - Wave Energy Harnessing Device [34]

cost of installation and transportation of this type of WEC is significantly less compared to the other models with massive structures and moving parts. Therefore, the point absorber type of WEC is chosen for this research. The dynamic modeling of the point absorber in the time-domain is discussed in the following section.

2.2 WEC Dynamics in the Time-Domain

A time-domain graph illustrates the changes to a signal over time, while a frequency-domain graph shows the existing deviation of the signal within a specific frequency range.

Usually for wind energy converters, analysis is performed in the time-domain since it allows for the direct inclusion of nonlinear time-varying factors such as power take-off reactions, mooring forces, and viscous drag [39]. Therefore, in order to account for the aforementioned time-varying factors in wave energy converters, this thesis includes the time-domain modeling.

2.2.1 Wave-Buoy Interaction

In this thesis, the WEC's structure consists of a floating buoy with rigid attachment to the end-effector of an open kinematic chain robot. The robot is deployed near-shore (approximately 5 km off the coastline). It is built specifically for converting heaving motion force

into translatory motion and pitching motion moment into rotary motion, as illustrated in Figure 2.7. The mechanics of the robot are discussed in detail in Chapter 4.

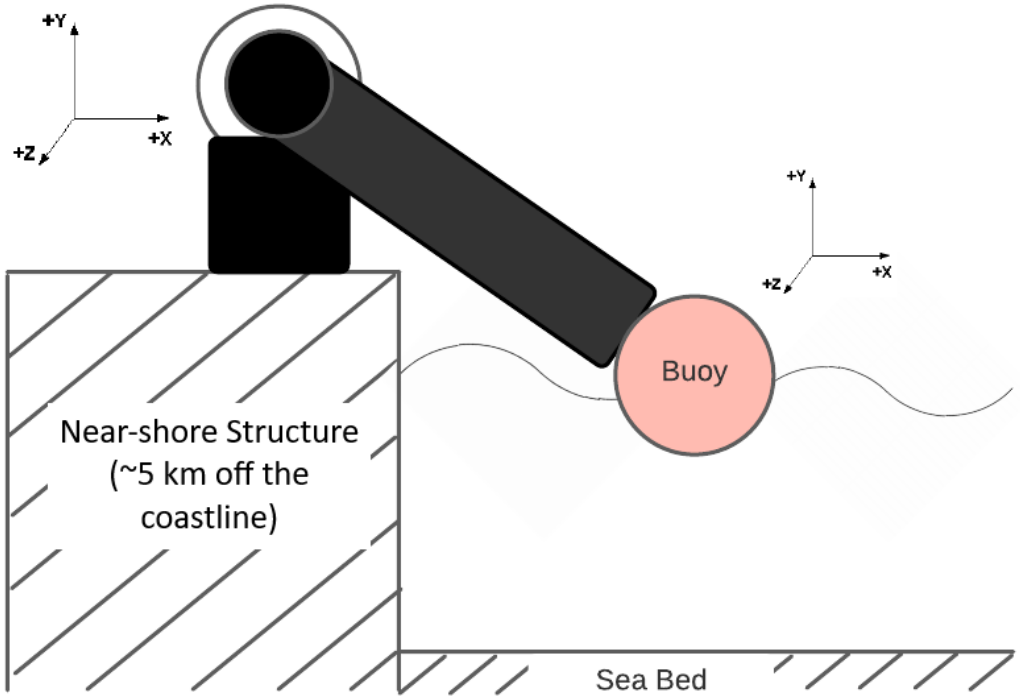

Figure 2.7: Proposed Wave Energy Converter Robotic System

When the advancement of waves moves the floating buoy upwards. The revolute and prismatic joint of the robot (attached rigidly to the buoy) rotates anti-clockwise and translates retracted respectively. Power transmission is accomplished through a linear generator attached to the prismatic joint and a rotary generator attached to the revolute joint. To be able to transmit maximum power, the control of the WEC model is necessary. The model formulations are done for six degrees-of-freedom, but in the case study of this thesis it has been limited to two: the heave, the z-movement and the pitch, the rotation around the y-axis. The buoy is connected to the arm rigidly, therefore it is assumed that there is no slippage between the arm and surface of the buoy (i.e., both move with the same velocity), the arm is in tension but does not stretch. It is also assumed that restoring components are zero when buoy position is zero or robot arm is in default position (reference plane x_0, y_0, z_0).

In the WEC simulation software called WEC-Sim [40], the equation of motion for a floating body about its center of gravity can be given as [41]:

$$M\ddot{X} = F_e(t) + F_{md}(t) + F_{rad}(t) + F_{PTO}(t) + F_v(t) + F_{me}(t) + F_B(t) + F_m(t) \tag{2.1}$$

where $\ddot{X}$ is the (translational and rotational) acceleration vector of the device, M is the mass matrix, $F_e(t)$ is the wave excitation force and torque (6-element) vector, $F_{md}(t)$ is the mean drift force and torque vector, $F_{rad}(t)$ is the force and torque vector resulting from wave radiation, $F_{PTO}(t)$ is the PTO force and torque vector, $F_v(t)$ is the damping force and torque vector, $F_{me}(t)$ is the Morison Element force and torque vector, $F_B(t)$ is the net buoyancy restoring force and torque vector, and $F_m(t)$ is the force and torque vector resulting from the mooring connection.

The forces $F_e(t)$, $F_{rad}(t)$ and $F_B(t)$ are calculated using hydrodynamic coefficients provided by the frequency-domain Boundary Element Method (BEM) solver. The radiation term includes an added-mass term, matrix $A(\omega)$, and wave damping term, matrix $B(\omega)$, associated with the acceleration and velocity of the floating body, respectively, and given as functions of radian frequency (ω) by the BEM solver. The wave excitation term $F_e(\omega)$ includes a Froude-Krylov force component generated by the undisturbed incident waves and a diffraction component that results from the presence of the floating body. The buoyancy term $F_B(t)$ depends on the hydrostatic stiffness K_{hs} coefficient, displacement of the body, and its mass. $F_{rad}(t)$ for this research is calculated using sinusoidal steady-state response scenarios. This method of calculation is often used for simple WEC designs with regular incoming waves. The radiation term can be calculated using the added mass and the wave radiation damping term for a given wave frequency, which is obtained from

$$F_{rad}(t) = -A(\omega)\ddot{X} - B(\omega)\dot{X} \tag{2.2}$$

where $\dot{X}$ is the velocity vector of the floating body, $A(\omega)$ is the added mass matrix, and $B(\omega)$ is the radiation damping matrix.

However, a simplified WEC dynamic equation is considered for the control theory formulation in this research. The motions of a point absorber are cyclic, and their response depends on the exciting wave's frequency [42]. At wave frequencies corresponding to the WEC's natural frequency, motions are more pronounced, and if harvested suitably, maximum power can be generated [43]. The wave – WEC interaction of forces in the time-domain also resembles a mass-spring-damper system [44, 45, 46]. In order to simplify the model, the frequency dependence of the hydrodynamic damping and the added mass have been neglected. In this case the dynamic model can be written in the form [47]:

$$[M + A_h]\ddot{X} + B\dot{X} + CX = F_e + F_R \tag{2.3}$$

where $\ddot{X}(t), \dot{X}(t)$ and $X(t)$ are the floating buoy's acceleration, velocity, and displacement vectors respectively in the time-domain. $[M + A_h]$ is the mass matrix plus the added mass matrix. The frequency independent hydrodynamic added mass and inertia act like additional mass in the system and is expressed as A_h. The wave excitation force and moment exerted on the buoy is abbreviated as $F_e(t)$ and the external end-effector force of the robot-buoy interaction as $F_R(t)$. The generalized spring coefficient or hydrostatic stiffness coefficient is conveyed by the C term and B is the radiation damping coefficient.

For n DOF, forces and motions are vectors with n terms; excitation coefficients that convert wave elevation into excitation forces and momentss are n $\times$ 1 vectors, while impedance coefficients that transform motions into forces are n $\times$ n matrices as shown in the following section.

2.2.2 6 DOF WEC Model

Six DOF of buoy motions (pitch, heave, roll, surge, sway, and yaw) are similar to ship/ float motions in the ocean. The movements induced by sea waves are classified by motion into two categories, translational and rotary. As Figure 2.8 illustrates the distinctions and axes, the dynamic equation of WEC can be expanded in matrix form as

$$X^T = \begin{bmatrix} s_x & s_y & h & r_x & \theta_p & y_z \end{bmatrix} \tag{2.4}$$

$$\dot{X}^T = \begin{bmatrix} \dot{s_x} & \dot{s_y} & \dot{h} & \dot{r_x} & \dot{\theta_p} & \dot{y_z} \end{bmatrix} \tag{2.5}$$

$$\ddot{X}^T = \begin{bmatrix} \ddot{s_x} & \ddot{s_y} & \ddot{h} & \ddot{r_x} & \ddot{\theta_p} & \ddot{y_z} \end{bmatrix} \tag{2.6}$$

where s_x is surge, s_y is sway, H is heave, r_x is roll, θ_p is pitch and y_z is yaw. These are the six degrees-of-freedom of the rigid-body.

$$A_h = \begin{bmatrix} A_{1,1} & A_{1,2} & A_{1,3} & A_{1,4} & A_{1,5} & A_{1,6} \\ A_{2,1} & A_{2,2} & A_{2,3} & A_{2,4} & A_{2,5} & A_{2,6} \\ A_{3,1} & A_{3,2} & A_{3,3} & A_{3,4} & A_{3,5} & A_{3,6} \\ A_{4,1} & A_{4,2} & A_{4,3} & A_{4,4} & A_{4,5} & A_{4,6} \\ A_{5,1} & A_{5,2} & A_{5,3} & A_{5,4} & A_{5,5} & A_{5,6} \\ A_{6,1} & A_{6,2} & A_{6,3} & A_{6,4} & A_{6,5} & A_{6,6} \end{bmatrix} \tag{2.7}$$

$$B = \begin{bmatrix} B_{1,1} & B_{1,2} & B_{1,3} & B_{1,4} & B_{1,5} & B_{1,6} \\ B_{2,1} & B_{2,2} & B_{2,3} & B_{2,4} & B_{2,5} & B_{2,6} \\ B_{3,1} & B_{3,2} & B_{3,3} & B_{3,4} & B_{3,5} & B_{3,6} \\ B_{4,1} & B_{4,2} & B_{4,3} & B_{4,4} & B_{4,5} & B_{4,6} \\ B_{5,1} & B_{5,2} & B_{5,3} & B_{5,4} & B_{5,5} & B_{5,6} \\ B_{6,1} & B_{6,2} & B_{6,3} & B_{6,4} & B_{6,5} & B_{6,6} \end{bmatrix} \tag{2.8}$$

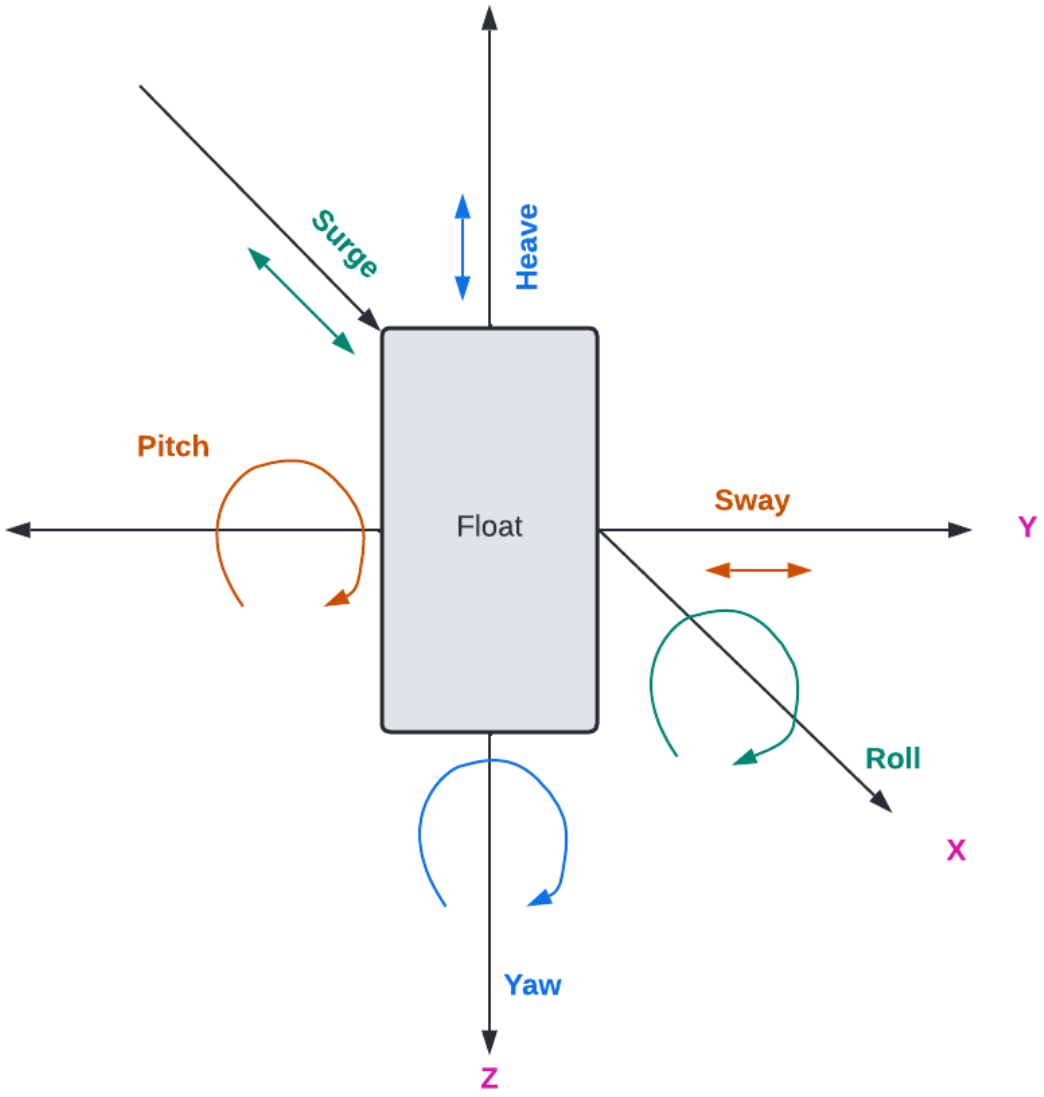

Figure 2.8: 6 Degrees-of-Freedom of a Floating Rigid-Body

$$C = \begin{bmatrix} C_{1,1} & C_{1,2} & C_{1,3} & C_{1,4} & C_{1,5} & C_{1,6} \\ C_{2,1} & C_{2,2} & C_{2,3} & C_{2,4} & C_{2,5} & C_{2,6} \\ C_{3,1} & C_{3,2} & C_{3,3} & C_{3,4} & C_{3,5} & C_{3,6} \\ C_{4,1} & C_{4,2} & C_{4,3} & C_{4,4} & C_{4,5} & C_{4,6} \\ C_{5,1} & C_{5,2} & C_{5,3} & C_{5,4} & C_{5,5} & C_{5,6} \\ C_{6,1} & C_{6,2} & C_{6,3} & C_{6,4} & C_{6,5} & C_{6,6} \end{bmatrix} \tag{2.9}$$

$$M = \begin{bmatrix} m & 0 & 0 & 0 & -zG & -yG \\ 0 & m & 0 & -zG & 0 & -zG \\ 0 & 0 & m & yG & -xG & 0 \\ 0 & zG & yG & I_{xx} & I_{xy} & I_{xz} \\ zG & 0 & zG & I_{yx} & I_{yy} & I_{yz} \\ -yG & xG & 0 & I_{zx} & I_{zy} & I_{zz} \end{bmatrix} \tag{2.10}$$

where m is the dry mass of the rigid-body, xG, yG and zG are the coordinates of the center of gravity and I_{ij} are the rigid-body moments of inertia. The WEC system includes the buoy but also has a robot dynamic aspect which is discussed in the following section.

2.2.3 WEC-Buoy Dynamics

In this research, the WEC system is considered to be a point absorber that functions similar to an open kinematic chain robot [48]. Therefore, the WEC dynamic equation is similar to robot dynamics expressed as follows

$$M(q)\ddot{q} + V(q,\dot{q}) + G(q) = \tau_{PTO} - J_R(q)^T F_R \tag{2.11}$$

where M(q) is the robot's generalized mass matrix; $q, \dot{q}, \ddot{q}$ are the generalized position, velocity, and acceleration vectors of joints, $V(q,\dot{q})$ is the Coriolis and centrifugal terms and $G(q)$ is the gravitational term; τ_{PTO} is the external generalized forces of the robot, $F_R(t)$ is the interaction force of the robot and buoy and $J_R(q)$ is the robot Jacobian.

The robot dynamic equations with respect to the joint variables cannot be combined with the WEC dynamic equation directly as the robot equation must first be converted with respect to the buoy acceleration, buoy velocity, and buoy position ($\ddot{X}, \dot{X}$ and X respectively) [48]. This is done by converting the robot dynamic equation to the same Cartesian plane as the buoy. The Jacobian corresponding to the Cartesian external forces of the robot is abbreviated as $J_R(q)^T$. The equations are obtained using the Jacobian relationship and robot dynamic equations in Cartesian form as follows [49]

$$\dot{X} = J_R(q)\dot{q} \tag{2.12}$$

$$\ddot{X} = \dot{J_R}(q)\dot{q} + J_R(q)\ddot{q} \tag{2.13}$$

$$X = f(q) \tag{2.14}$$

Therefore, the robot dynamic equations in Cartesian form is given as.

$$M_x(q)\ddot{X} + V_x(q,\dot{q}) + G_x(q) = J_R(q)^{-T}\tau_{PTO} - F_R \tag{2.15}$$

where

$$M_x(q) = J_R(q)^{-T} M(q) J_R(q)^{-1} \tag{2.16}$$

$$V_x(q, \dot{q}) = J_R(q)^{-T} V(q, \dot{q}) - M_x(q) \dot{J_R}(q) \dot{q} \tag{2.17}$$

$$G_x(q) = J_R(q)^{-T} G(q) \tag{2.18}$$

Hence, from (2.15) and equation (2.3) we have,

$$M_x(q)\ddot{X} + V_x(q, \dot{q}) + G_x(q) = J_R(q)^{-T} \tau_{PTO} - ([M + A_h]\ddot{X} + B\dot{X} + CX - F_e(t)) \tag{2.19}$$

where

$$J_R(q)^{-T} \tau_{PTO} = F_{PTO} \tag{2.20}$$

Equation (2.19) is the WEC dynamic equation including both buoy and robot dynamics. This equation is the baseline for the power maximizing conditions found in the next chapter and the case study explored in Chapter 4.

2.3 Conclusion

In this chapter, a review of the various types of wave energy converters are explored, and the hydrodynamics of a point-absorber type wave energy converter is detailed. The second half of this chapter includes the dynamic interaction between the sea state, the buoy and the WEC. The dynamic model is described in the time-domain. A simple mass-spring-damper system in the time-domain is used to analyze the forces acting on the buoy and the overall system is accounted for using robotic concepts.

Chapter 3

Power-Maximizing Controller

One of the main objectives of this dissertation is to extract maximum power from the waves. However, variations in the wave patterns can lead to variation in power capture. To counteract the variations of the ocean environment, a control algorithm is necessary. In order to achieve maximum power absorption, the WEC system needs to be a good wave-maker, i.e., the velocity of the WEC and excitation force/ moment need to be in phase, while the position of the WEC and excitation force/ moment need to be out of phase.

3.1 Review of Current Control Strategies

WEC control generally aims to maximize captured energy while relying on feed-forward control to generate good mounting speeds or PTO force settings. Many strategies for controlling the power take-off system of wave energy converters have been proposed and investigated. In the early 1970s, Budal and Falnes [50] examined both reaction control and latching control [51]. They carried out much of the initial development of latch-type "phase control" through both theory and wave tank experiments [52].

Research over the last two decades has addressed model predictive control (MPC) [53] for WECs. Some researchers also provided a comparative study between several prediction-model based control systems [54]. Majority of the control strategies described here use optimization algorithms. Optimization is either implemented when designing a control strategy (that is, to determine some essential gain factors) or when determining the control signal during execution. Proportional linear quadratic control [55], and proportional-derivative based complex conjugate control [56] use optimization in the control design. Model predictive control mentioned above, moment-based control [57], and dynamic programming [58] use optimizations to select control signals during execution. Almost all the research for WEC control always results in a key factor – resonance. When operating in resonance, the response amplitude is maximized. Therefore, it is necessary to resonate the system with tuning the PTO damping and stiffness parameters as needed to draw maximum power from the waves.

In this research, the objective is to maximize the wave power absorption by actively controlling system parameters on the basis of a WEC dynamic model in the time-domain. A sliding-mode control (SMC) algorithm is proposed to be implemented with an extremum seeking function. SMC provides unique advantages for dealing with model uncertainty and disturbances. It is widely used in aerospace engineering, marine engineering, and other power generation fields. Additionally, an extremum seeking algorithm [59] that uses a sliding mode to find the target value that leads to the extremum is introduced. The error function of the extremum seeking algorithm remains within a range by decreasing in the sliding mode, until the extremum is maximized. The proposed extremum seeking algorithm [60] should guarantee satisfactory control performance irrespective of how the system parameters change. The conditions at which the proposed SM-ES controller maximizes power absorption is found in the next section.

3.2 Derivation of Conditions for Maximum Power Transfer

As mentioned previously, the proposed WEC's velocity must be forced to be in resonance with the wave excitation force/ moment to absorb maximum energy. The controller is designed to compensate for the non-linearity and the changing mass matrix when multiple degrees-of-freedom are considered. Let us take F_{PTO} (refer to equation (2.20)) as a feedback linearizing controller in the WEC dynamic equation (2.19) as follows,

$$F_{PTO} = V_x(q, \dot{q}) + G_x(q) + U \tag{3.1}$$

where U is the new input to the robot's controller equation which is defined later in this section. It will be shown through simulations that the feedback linearization controller uses a fraction of the overall absorbed energy. An intuitive justification of the above result is that the Coriolis, centrifugal, and gravitational forces are relatively small with respect to wave excitation forces and moments due to the relatively slow motion of the WEC system and the equilibrium gravity force balanced by the buoyancy force, respectively. The power consumed to linearize the system is calculated from equation (3.1) by multiplying $\dot{X}$ on both sides as

$$F_{PTO}\dot{X} = [V_x(q, \dot{q}) + G_x(q)]^T \dot{X} + U^T \dot{X} \tag{3.2}$$

Then the energy consumed (E_c) over a time interval [0 t] can be computed as:

$$E_c(t) = -\int_0^t [V_x(q, \dot{q}) + G_x(q)]^T \dot{X}\, d\tau \tag{3.3}$$

The actual energy consumed by the feedback linearization controller is presented later in the controller simulation results section of Chapter 5. The WEC dynamic equation (2.19)

with the new input to the system becomes

$$M_x(q)\ddot{X} = U - ([M + A_h]\ddot{X} + B\dot{X} + CX - F_e(t)) \tag{3.4}$$

Hence

$$[M_x(q) + M + A_h]\ddot{X} + B\dot{X} + CX = U + F_e(t) \tag{3.5}$$

Defining

$$M_T = M_x(q) + M + A_h \tag{3.6}$$

and rearranging (3.5) we have

$$M_T\ddot{X} + B\dot{X} + CX - F_e(t) = U \tag{3.7}$$

Now, given this new input U and considering equation (3.7) as the new system, the extracted energy over a time interval [0 t] can be computed as:

$$E(t) = -\int_0^t \dot{X}^T U \, d\tau \tag{3.8}$$

In the above equation, replacing U from (3.7) gives

$$E(t) = -\int_0^t \dot{X}^T [M_T(\tau)\ddot{X} + B\dot{X} + CX - F_e(\tau)] \, d\tau \tag{3.9}$$

Integrating the equation becomes

$$E(t) = -\frac{1}{2}\dot{X}^T M_T \dot{X} - \frac{1}{2}X^T CX + \frac{1}{2}\dot{X_0}^T M_T \dot{X_0} + \frac{1}{2}{X_0}^T C X_0 + \int_0^t \dot{X}^T (F_e(t) - B\dot{X}) \, d\tau \tag{3.10}$$

Now let

$$F_e(t) - B\dot{X} = P\dot{X} \tag{3.11}$$

where P is a positive definite matrix. Then, the energy captured in (3.10) can be re-written as

$$E(t) = E_0 - \frac{1}{2}\dot{X}^T M_T \dot{X} - \frac{1}{2}X^T CX + \int_0^t \dot{X}^T P\dot{X} \, d\tau \tag{3.12}$$

where the initial energy term is

$$E_0 = \frac{1}{2}\dot{X_0}^T M_T \dot{X_0} + \frac{1}{2}{X_0}^T C X_0 \tag{3.13}$$

It is observed from (3.12) that when in motion if the norm of the matrix P is maximized, the integral term is maximized resulting in the energy (E) also being in the maximum range. The range within which the norm of the matrix P is maximized, and the energy term is positive is called as maximum range in this research. From equation (3.11), we observe that the speed of the system influences the P term. Hence, the desired speed for efficient power

transfer when the WEC is in motion can be found by rearranging (3.11) as follows

$$\dot{X} = (B + P)^{-1} F_e(t) \tag{3.14}$$

The energy equation (3.12) can then be re-written to accommodate the desired speed as follows

$$E(t) = E_i + \int_0^t F_e(t)^T (B + P)^{-1} P (B + P)^{-1} F_e(t)\, d\tau \tag{3.15}$$

where

$$E_i = E_0 - \frac{1}{2}\dot{X}^T M_T \dot{X} - \frac{1}{2} X^T C X \tag{3.16}$$

Using matrix norm inequalities as follows

$$E(t) < E_i + \int_0^t \frac{||P||}{(||P|| + ||B||)^2} F_e(t)^T F_e(t)\, d\tau \tag{3.17}$$

The term $\frac{||P||}{(||P||+||B||)^2}$ is maximized when $||P|| = ||B||$. Now referring to (3.14), for a *usually unknown* $F_e(t)$ and B, the desired speed $\dot{X}_d$ is the one that maximizes E. To obtain $\dot{X}_d$ in real time, we propose using an extremum seeking method. To this end, utilizing (3.15), let us define an average power term as follows

$$P_{avg} = \lim_{T \to \infty} \frac{E(T)}{T} \tag{3.18}$$

The desired speed $\dot{X}_d$ needs to be obtained at each instant such that one always moves in the direction of maximizing the net power P_{avg}. Thus, P_{avg} can be considered to be a function of $\dot{X}$ with the extremum seeking controller determining desired $\dot{X}$ in the direction of reaching the maximum at each instant. The acceleration, $\ddot{X}$ can be obtained by re-arranging the system equation (3.7) as follows

$$\ddot{X} = M_T^{-1}(U - B\dot{X} - CX + F_e(t)) \tag{3.19}$$

Now defining $\sigma = \dot{X}_d - \dot{X}$, $\dot{\sigma}$ can be obtained by

$$\dot{\sigma} = \ddot{X}_d - \ddot{X} \tag{3.20}$$

Then, replacing $\ddot{X}$ from equation (3.19) we obtain $\dot{\sigma}$ as follows

$$\dot{\sigma} = \ddot{X}_d - M_T^{-1}(U - B\dot{X} - CX + F_e(t)) \tag{3.21}$$

Furthermore, let the new input U be taken as

$$U = K_B \dot{X} + K_C X + M_T(\ddot{X}_d + K_\sigma \sigma) \tag{3.22}$$

where K_B, K_C, and K_σ are positive-definite gain matrices. Then replacing U from equation (3.22) in equation (3.21) we get

$$\dot{\sigma} = \ddot{X}_d - M_T^{-1}([K_B\dot{X} + K_C X + M_T(\ddot{X}_d + K_\sigma\sigma)] - B\dot{X} - CX + F_e(t)) \tag{3.23}$$

Solving further we get

$$\dot{\sigma} = \ddot{X}_d - M_T^{-1}((K_B - B)\dot{X} + (K_C - C)X + M_T\ddot{X}_d + M_T K_\sigma\sigma + F_e(t)) \tag{3.24}$$

Then, continuing to solve we obtain

$$\dot{\sigma} = \ddot{X}_d - [M_T^{-1}(K_B - B)\dot{X} + M_T^{-1}(K_C - C)X + \ddot{X}_d + K_\sigma\sigma + M_T^{-1}F_e(t)] \tag{3.25}$$

The equation is then re-arranged as

$$\dot{\sigma} = \ddot{X}_d - \ddot{X}_d - K_\sigma\sigma + M_T^{-1}[(B - K_B)\dot{X} + (C - K_C)X - F_e(t)] \tag{3.26}$$

The above equation is further simplified as

$$\dot{\sigma} = -K_\sigma\sigma + M_T^{-1}[(B - K_B)\dot{X} + (C - K_C)X - F_e(t)] \tag{3.27}$$

and re-arranging equation (3.27) we have

$$\dot{\sigma} + K_\sigma\sigma = M_T^{-1}[(B - K_B)\dot{X} + (C - K_C)X - F_e(t)] \tag{3.28}$$

Therefore, when $\dot{\sigma} + K_\sigma\sigma = 0$, the desired speed matches the actual speed. i.e. $\sigma = 0$. Then we have

$$\begin{aligned} \dot{\sigma} + [K_\sigma + M_T^{-1}(B - K_B)]\sigma + M_T^{-1}(C - K_C)\int_0^t \sigma \\ = \quad M_T^{-1}[(B - K_B)\dot{X}_d + (C - K_C)X_d - F_e] \end{aligned} \tag{3.29}$$

Now for finite X_d, $\dot{X}_d$ and F_e, appropriate selection of gains K_σ, K_B, and K_C (e.g., gains that render the coefficients of σ and $\int\sigma$ positive definite), would force the term σ to converge to small values. Hence, $\dot{X} \to \dot{X}_d$ where $\dot{X}_d$ is found by an extremum seeking controller in which the input parameter of the ESC scheme is the average power P_{avg} (e.g., can be calculated using the voltages and currents) and output parameter is $\dot{X}_d$. This will be discussed further in the following section.

The power consumed by the feedback linearizing controller (3.1) to linearize the non-linear WEC system is shown later in Chapter 5.

3.3 Proposed Control

3.3.1 Sliding Mode Extremum Seeking Control

Control, in terms of this research, refers to the adaptation of the wave energy converter to behave in resonance over a multi-frequency regular waveform. To enhance the robustness of the model while simultaneously maximizing energy output, this study proposes the implementation of an adaptive controller using sliding mode (SM) based ES control strategy [17]. The WEC controller is discussed further in terms of the 2 DOF WEC case study in Chapter 4.

The objective function (as shown in Figure 3.1) is to maximize $y(t) = P_{avg}(\dot{X})$. From the paper, the sliding-surface function α of the proposed controller for WEC system is given as

$$\alpha = P_{avg}(\dot{X}) - g(t) \tag{3.30}$$

where $\alpha(t)$ is the sliding-surface vector generated that maximizes the power by tracking the output of the system, $P_{avg}(\dot{X})$ alongside a time increasing function $g(t)$. The gradient of the time increasing function, also known as driving function, is expressed as

$$\dot{g}(t) = \rho \tag{3.31}$$

where ρ is a driving signal which is always a positive constant. For $\rho > 0$ in a maximization problem as such

$$\dot{\alpha} = \frac{dP_{avg}}{d\dot{X}}\ddot{X} - \dot{g}(t) \tag{3.32}$$

The selection of an adequate driving vector ρ enables the controller to reach the sliding-surface for the maximization problem. In order to remain in the maximum range once the sliding-surface is reached, the controller includes a switching function that enables the sliding surfaces to maintain in the maximum range. Real value functions are determined by the Signum function. These real values can be used to find the direction in which the system is maximized. Therefore, switching is done as in the paper referenced by feeding the sliding-surface function error to a signum (sgn) function with the control optimization law as follows:

$$\dot{X}_d = Ksgn[sin(\frac{\pi\alpha}{\epsilon})] \tag{3.33}$$

where ϵ is a 1 $\times$ n vector for which each element is a positive constant, K is an n $\times$ n diagonal positive definite matrix which determines the convergence rate and the signum function is a period switching signal since the performance function cannot be predicted for multiple frequency regular waves. The period switching signal will determine the direction

of the system and switch the direction accordingly to maintain maximum power by forcing $P_{avg}(\dot{X})$ to remain on the increasing sliding-surface vector, ensuring error is minimum, i.e. $\alpha(t) \to 0$. The Sine operator which is used in the signum function, helps the ESC algorithm to find the correct direction in which the objective function is maximized. Moreover, α defines the desired speed $\dot{X}_d$, also the bound on the error that is allowed by the system.

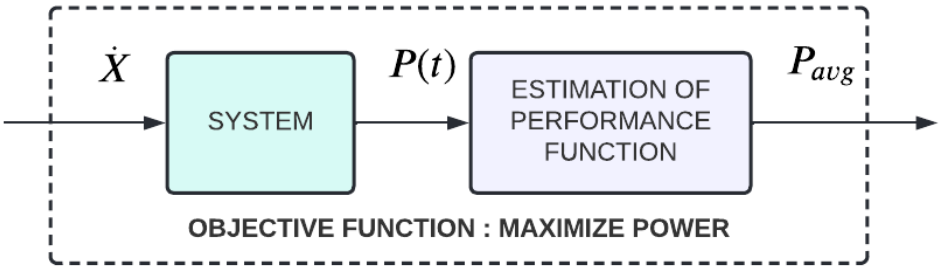

Figure 3.1: Block Diagram of the Objective Function in the Proposed Sliding Mode Extremum Seeking Controller

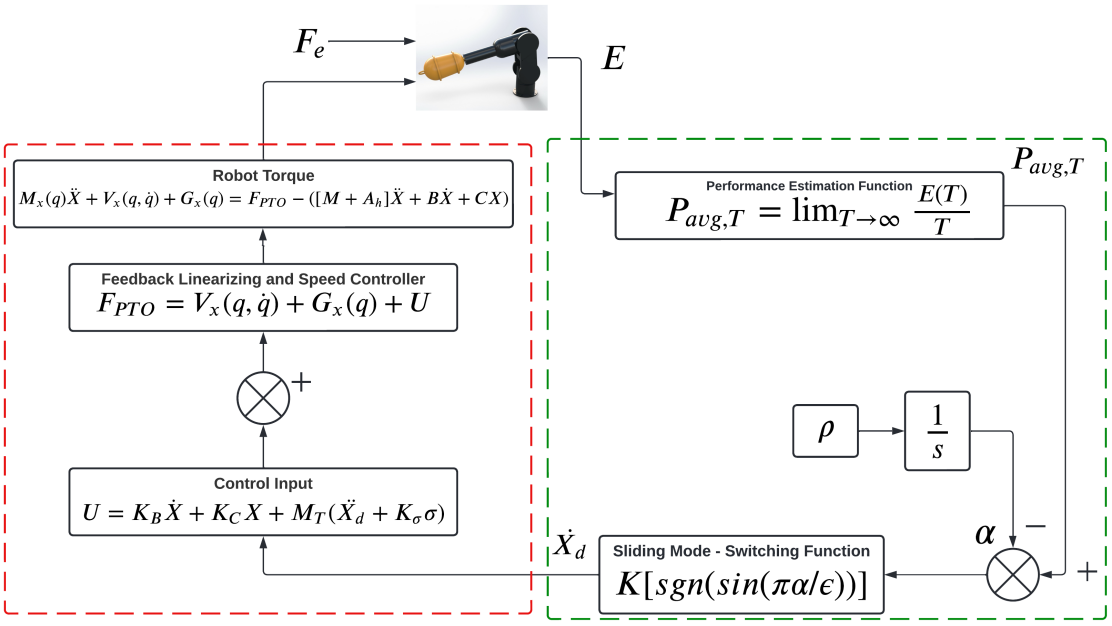

Figure 3.2: Workflow of the Proposed Sliding Mode Extremum Seeking Controller with Maximum Power Transfer Function

The basic idea of this controller is to make P_{avg} follow an increasing/decreasing time function via sliding-modes. The output of the WEC system is the instantaneous power $P(t)$,

which is characterized by high as well as low frequency contents, but only at lower values can it be characterized by the slow variation of the parameter provided by the switching function of the SM-ES observer (see Figure 3.2). However, the system is subject to variations (such as changing wave heights or periods) which results in different magnitudes of power. As such, the logarithmic function is used to significantly reduce the differences in performance metrics, reducing the requirement to continuously re-tune ES hyperparameters as operating conditions change. The following Figure 3.3 portrays the estimation of the performance function.

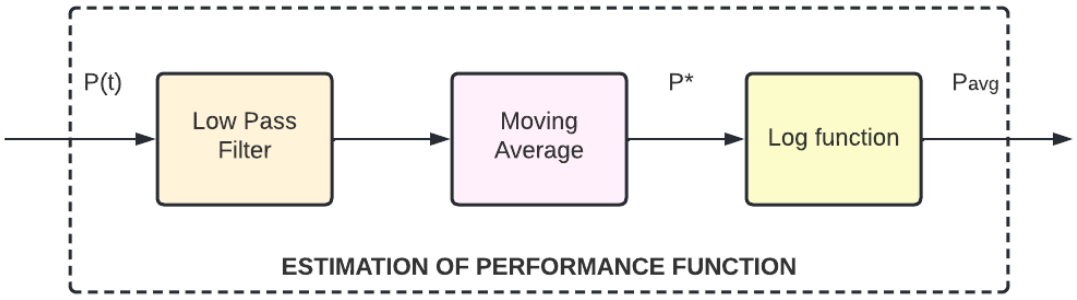

Figure 3.3: Block Diagram of the Performance Function Estimator in the Proposed Sliding Mode Extremum Seeking Controller

The most important innovations and contributions of this research are condensed as follows:

- WEC model's output variations are dealt with in the sliding mode used in the extremum seeking controller.
- The strategy is in the time-domain, is adaptive and a model-free approach. The controller is adaptive with respect to its ability to adapt and find maximum power with a multi-frequency regular wave input. Future work could include the possibility of testing this control scheme with irregular wave input. It is a model-free approach as it doesn't require prediction models and exact model of the system isn't required to find maximum power.
- The proposed controller has a low execution time per time step, during simulation as it doesn't require pre-processing prediction models. The feedback linearization controller also eliminates the need for continuously linearizing the non-linear WEC system.
- The adjustment procedure is simple because the approach has only 3 control parameters to be tuned. The control parameters are ρ and the two hyperparameters K and ϵ. The values of these parameters are tabulated in the next chapter.

In the Appendix of this thesis, Figure A.2 shows a zoomed image of Figure 3.2.

3.4 Latching Control

Wave energy converters use a latching control strategy to latch and unlatch moving parts successively. Using this approach, high velocities can be achieved, which in turn allows a large amount of energy to be captured. In latching control, the motion of a body is locked at the very moment its velocity ceases at the end of one oscillation, and waits for the most favorable situation to unlock the body. The estimation of how long the system remains locked is the problem to be solved.

3.4.1 Optimal Command Theory Latching Control

In this research, the WEC system's latching control is applied based on the optimal command method proposed [61]. The optimal command theory is based on Pontryagin's maximum principle which is implemented in control theory to find the best possible control for taking a non-linear system from one state to another, especially in the presence of constraints on the state or input parameters.

When latching control is implemented, an additional force must be applied in the dynamic of the WEC system to cancel the acceleration of the controlled motion. Moreover, latching control is implemented when the velocity is nearly zero, so during the locking phase, the equation of motion has:

$$\dot{X} = 0 \tag{3.34}$$

The latching theory is implemented as in the paper by formulating a weaker model of latching control as opposed to an absolute bang-bang latching strategy. During absolute latching control, a force is applied on the body that instantaneously stops the acceleration of the motion. When a weaker model is applied, the additional force is replaced by a very large (but not infinite) damping force. Therefore, it is possible to model latching control by adding a large robot control force (U) in the motion equation (3.5) as discussed in the paper as:

$$U = -Gl\dot{X} \tag{3.35}$$

where G is the (large) damping coefficient and l is the latching control variable. When l = 0, no latching control is applied; when l = 1, it is.

Following the formulations from the paper, we consider a sequence of wave excitations over a long duration [0, T]. Then, we can determine the binary sequence l(t) which maximizes the energy production as:

$$max_l E(l) = \int_0^T P(t, X, l)\, dt \tag{3.36}$$

where P(t, X, l) is the instantaneous power absorbed as in the referenced paper. Now, we assume as done in the paper, that the state of the system is given by a first order differential equation as:

$$\dot{X} = f(t, X, l) \tag{3.37}$$

Then, we can also define the Hamilton as in the paper referenced as:

$$H = P(t, X, l) + \lambda^t f \tag{3.38}$$

where $\lambda \in \mathbb{R}^n$ is the adjoint state vector and λ is derived by integrating the set of adjoint equations as:

$$\dot{\lambda_i} = -\frac{\partial H}{\partial X}(t, X, l) \tag{3.39}$$

The final condition can be considered as:

$$\lambda(T) = 0 \tag{3.40}$$

According to the Pontryagin maximum principle [62], the latching command l is responsible for the maximization of the Hamiltonian H at each time $t \in [0, T]$. An iterative process is used to calculate it in practice. The average power absorbed is given as

$$P_{avg} = \lim_{T \to \infty} \frac{max_l E(l)(T)}{T} \tag{3.41}$$

No control is applied at the beginning of the process. Then, the device motion is found by integrating equation (3.37) forward for $t \in [0, T]$. Once the motion has been computed, the adjoint state vector λ is found by backward integration, equation (3.39) from t = T to t = 0. Using X and λ, a new control algorithm $l(t)$ is deducted at each time step which maximizes the Hamiltonian, and then iterates the process.

The application of this strategy to the WEC system is explored in the following Chapter 4 and the results of the controller performance depicted in Chapter 5.

3.5 Conclusion

In this chapter, the conditions for maximum power transfer based on the dynamic equations obtained in the previous chapter are derived. After a quick review of current WEC control schemes, an SM-ES controller is proposed by defining a sliding surface for the controller. Then, a latching control is introduced as an alternative control algorithm. The performance of the proposed sliding-mode extremum seeking scheme and latching control algorithm will be further studied in the following chapters.

Chapter 4

Simulation Studies

4.1 Design of Floating Buoy

Marine buoys are versatile and used for several tasks, for example to measure weather variables such as wave height, wind speed, wind direction, swell period, swell direction, air temperature, water temperature, and barometric pressure. Buoys are also used for ship maneuvering, and coastal security. For instance, buoys can activate emergency alerts and warnings at densely populated coastal areas, cargo ships, aviation, fishing communities, underwater operations, and many other activities. Sensor-based ocean buoys are capable of real-time data collection and transfer, which is ideal for some above-mentioned tasks.

The design of a buoy is also an important aspect to the power absorption by the WEC robotic system, given that it would be the point of contact between the robot manipulator and the waves. In the first part of this chapter, the author discusses the wave climate chosen, followed by a brief explanation of the buoy and the robot design used in the simulation case study.

Review of Current Buoys in Marine Technology

In marine science, buoys are floating structures having a long history and various uses ranging from tracking changes in the oceanography and meteorology of the marine environment, as well as navigation, wave-measurement and storm warning systems [63, 64, 65, 66, 67]. More recently, certain buoy designs are automated to create robust systems that can operate in extreme depths, or in remote locations while allowing power and data connections to submerged instrumentation. The buoy's structure and size usually depend on the location where the buoy is deployed. Therefore, the next section discusses the selection of the deployment location for this dissertation's case study.

4.1.1 Wave Location

Based on a previous study [68], wave energy converter deployment in the near-shore is unlikely to be economically viable. This is due to the near-shore energy resource that appears

to be much smaller than the offshore energy resource when the average gross wave power density is used as a measure of the wave energy resource. This is often quoted as the main reason why wave energy converters should be located offshore in deep water, and possibly why the vast majority of wave energy converters are designed for deep water. There is an argument, however, that net wave energy resources are not necessarily the best way to determine the productivity of wave farms. In this thesis, one of the objectives is to deploy the simulated WEC at a near-shore location.

Location Selection

Wave profiles are typically milder close to the shoreline. However, maximum wave heights in near-shore areas are closer to average wave heights, which indicates that wave energy resources in near-shore areas can be exploited as those offshore. Generally, near-shore technologies are considered to have higher survivability and cost-effectiveness than offshore solutions [69]. This is primarily based on installation and maintenance aspects of the WEC system deployed. In Canada, the Vancouver Island coast is viewed as one of the attractive deployment locations for wave energy converters.

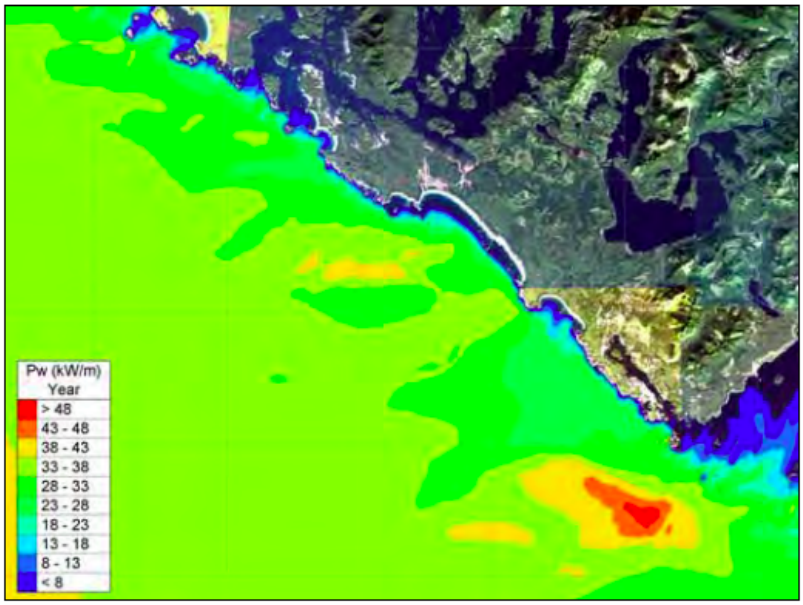

Figure 4.1: Annual Power (kW/m) at the Vancouver Island Coast [69]

Global wave energy [70] records have concluded after quantifying oceans all over the world that the west coast of Canada holds one of the most dynamic wave climates, with average yearly wave energy transport of <8 kW/m occurring at the Vancouver Island shoreline as illustrated in Figure 4.1.

The Marine Environmental Data Services (MEDS) station MEDS103 marked in Figure 4.2, is located at 41 m water depth ≈ 4.8 km off Wickaninnish Beach, Pacific Rim National Park. This is chosen as an ideal location for the system discussed in this paper. The average annual wave conditions are characterized by significant wave height (Hs) and peak period (Tp) which is 1-2.5 meters, 9-12 seconds for this location, respectively. For this research the significant wave height (Hs) and peak period (Tp) which are considered as 2.5 meters and 12 seconds respectively.

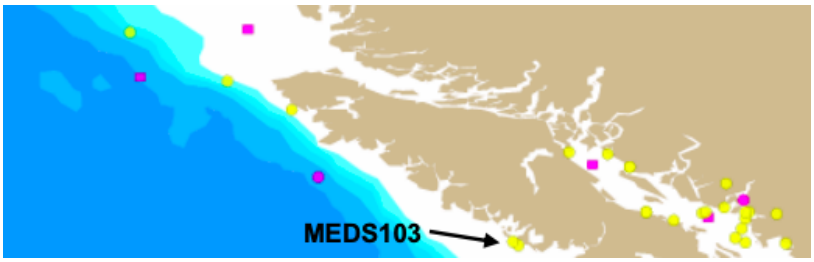

Figure 4.2: Location of the Marine Environmental Data Services station [69]

4.1.2 Buoy Shape Optimization

The buoy shape chosen is a truncated cone with a hemisphere attached to the base as shown in Figure 4.3. This is because the study shows that a spherical buoy leads to the most efficient power extraction in an annual wave energy spectrum [71] when compared to other shapes such as tulip or cylindrical.

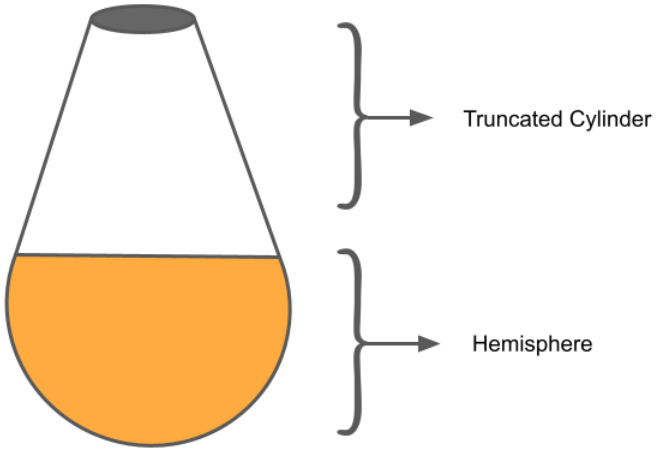

Figure 4.3: Buoy Shape: truncated cone Top and Hemisphere Base

The dimensions of the buoy for this research is designed depending on the wave climate at the WEC deployment location. The buoy's material is selected based on the best material commercially available buoys are made in compliance with the marine environment chosen. The buoy is also designed with curved edges to avoid corrosion and bio-fouling, as seen in Figure 4.4.

Figure 4.4: Case Study: Buoy Part Model

Buoy scaling

For maximizing power capture, a buoy's stroke length should be long. Long strokes demand larger WECs which are both economically and mechanically more challenging, while short strokes diminish power output. Point-absorbers, however, need some key characteristics to increase their energy absorption, one of which is to have a large stroke, preferably larger than the wave height range mentioned previously. A large stroke can be achieved by having a large robot control force that will enable the WEC's velocity to be in resonance with the wave excitation force/ moment, which is explored using the proposed control scheme and latching control method in Chapter 5. The dimensions of the buoy however must be

scaled with respect to the wave height of the waves of the chosen location. The significant wave height is 2.5 m for the desired location of extraction, therefore, the buoy designed will achieve a large stroke based on its height given in Table 4.1. A few dimensions of the buoy are also depicted in Appendix Figure A.1 of this thesis.

Buoy Material Selection

The most common plastic is polyethylene, and it is used to make buoys, toys, bulletproof vests and even air filters because of its strength, light weight, and versatility. Low-Density Polyethylene (LDPE) has greater tensile strength, exhibits high impact and puncture resistance compared to some other plastics, and is intentionally designed for rotational molding applications. It is chosen as the material for the custom buoy due to its toughness, flexibility, and minimal impact on the environment. The buoy may require less maintenance, as the LDPE material is colored with pigments that soak all the way through the polyethylene. The LDPE properties such as Young's Modulus, density, and other given material properties were used in the SolidWorks CAD environment to get the buoy properties tabulated in Table 4.1.

Buoyancy and Buoy Hydrodynamics

It is necessary to estimate the loads on buoys in order to make sure the overall structure can withstand the loads. This can be accomplished partly by considering the hydrostatic pressure on the buoy as well as by taking into account the end stop forces since the stroke length is limited.

When the buoy is immersed in seawater, its weight will pull it downwards. Buoyancy is the upthrust acting opposite to that weight, and has a magnitude directly proportional to the volume of the displaced fluid. The formula for calculating Buoyant force, B_f according to Archimedes principle is

$$B_f = \rho_d V g \tag{4.1}$$

where ρ_d is the fluid density (for seawater 1025 kg/m^3), V is the displaced volume of water and g is the gravitational acceleration set to 9.81 m/s^2. The parameters of the buoy are highlighted in the following Table 4.1. The mass of the displaced liquid is calculated to be 3718 kg. In comparison, the mass of the buoy is less than the mass of displaced liquid. Hence, theoretically it is proven that the buoy will float in the water as it is less dense than the ocean water.

4.1.3 Buoy Properties

The summarized buoy characteristics are in Table 4.1.

Characteristic Name	Value
Buoy Radius	1.3274 m
Buoy Height	6 m
Buoy Mass	2901.635 kg
Buoy Material	Low-Density Polyethylene (LDPE)
Buoy Density	800 $kg/_{m^3}$
Displaced Volume (V)	3.627 m^3
Sea Water Density (ρ_d)	1025 $kg/_{m^3}$
Mass of Sea Water Displaced	3718 kg

Table 4.1: Wave and Buoy Specifications

4.2 Design of 2 DOF WEC System

Generally, on a buoy there is a wave excitation force/ moment and several other forces acting on it as represented in equation 2.1. There are also added mass and wave radiation forces due to the buoy's motion caused by the waves. These force components are based on the direction of motions namely heave, sway, surge, pitch, yaw, and roll [72]. The idea to harness energy from multiple DOF's is an objective in this research. Therefore, multiple wave motion force components are considered, specifically heave forces and pitch moments. The selection criteria for the robot manipulator are based on the selected direction of forces.

4.2.1 Robotics in Wave Energy Converters

Automation is the trend of the millennia, in which robotics is rapidly overtaking critical operations especially in harsh environments both on Earth and in Space. The powerful waves produced in oceans as a result of winds are a valuable resource that should be utilized to harvest energy. Recent studies display impactful robotic applications integrated into the field of wave energy conversion [73, 74, 75, 76].

The robotic system designed in this research acts primarily as a point absorber type WEC. The robot was designed as a 2 DOF open kinematic chain to host the buoy connected rigidly to it. The manipulator is designed with two distinct joints – one prismatic and one revolute, to intentionally capture the translatory motion (heave) and the rotary motion (pitch) of the buoy simultaneously to extract power using electrical machines. These machines can be rotary and linear motors or generators.

The joints can operate in modes: passive (translating motion) and dynamic (using motors/generators to translate as well as apply control to the system). If a joint is connected to a motor, it consumes electricity but if a joint is connected to a generator it produces electricity. In this research, we consider joints connected to generators in dynamic mode. When dynamically enabled, a joint can be free or controlled in force/torque, in velocity or in position. This research therefore uses two independent joints operated dynamically in force/torque control mode [77].

Additionally, the use of an electrical machine as a PTO system for a WEC provides the possibility of directly converting mechanical energy into electrical energy. This can be visualized in Figure 4.5.

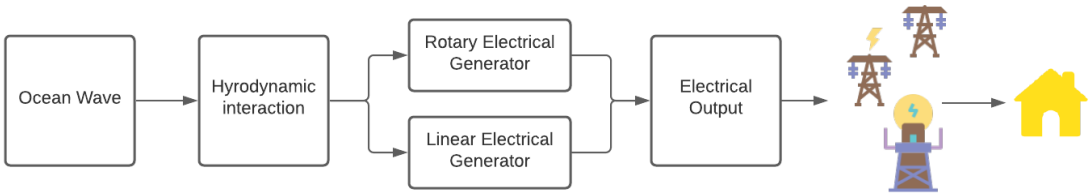

Figure 4.5: Flowchart showing the conversion of wave energy to electricity through a Direct Power take-off system

Figure 4.6 illustrates the preliminary design of the robot and its joints. The revolute joint near the robot's base is near-shore (approximately 5 km off the coastline) and the prismatic joint in motion with the end-effector attached rigidly to the buoy in the ocean. The joint's trajectory of movements is also depicted in the image using arrows.

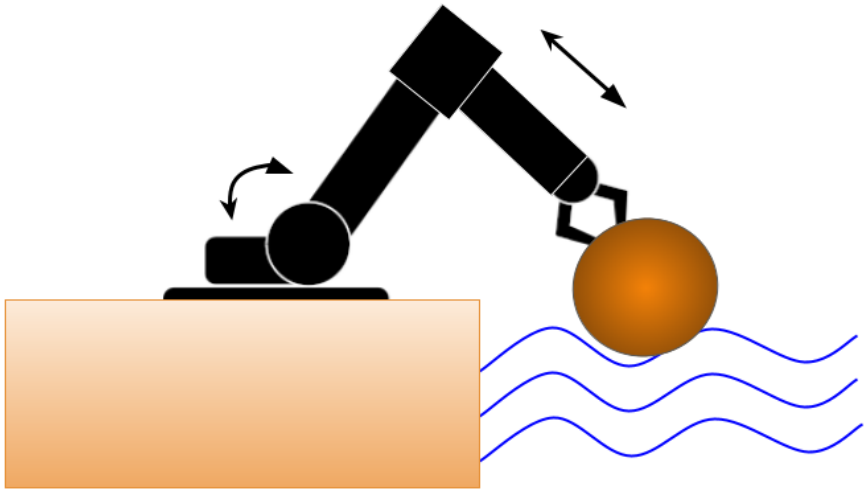

Figure 4.6: Conceptual Design of Wave Energy Converter Robotic System. The robot base in this image is assumed to be placed near-shore (approximately 5 km off the coastline).

4.2.2 Rotary Joint

Joints with a rotary feature have one DOF and are used to describe rotational movements. These movements are described by a single value which represents the amount of rotation about the first reference frame. Figure 4.7 and 4.8 are based on when the rotary joint is moved anti-clockwise and clockwise respectively. The figures show the joint orientation in the WEC assembly.

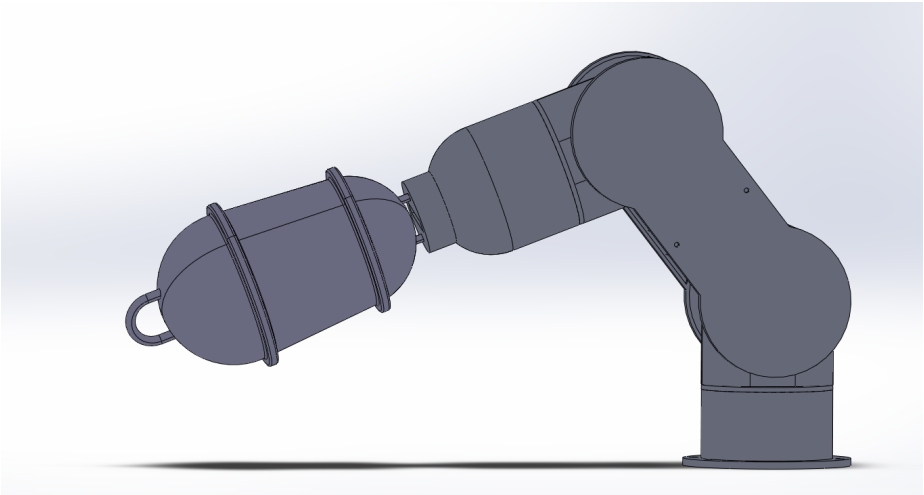

Figure 4.7: Rotary Joint Motion in Anti-clockwise Direction

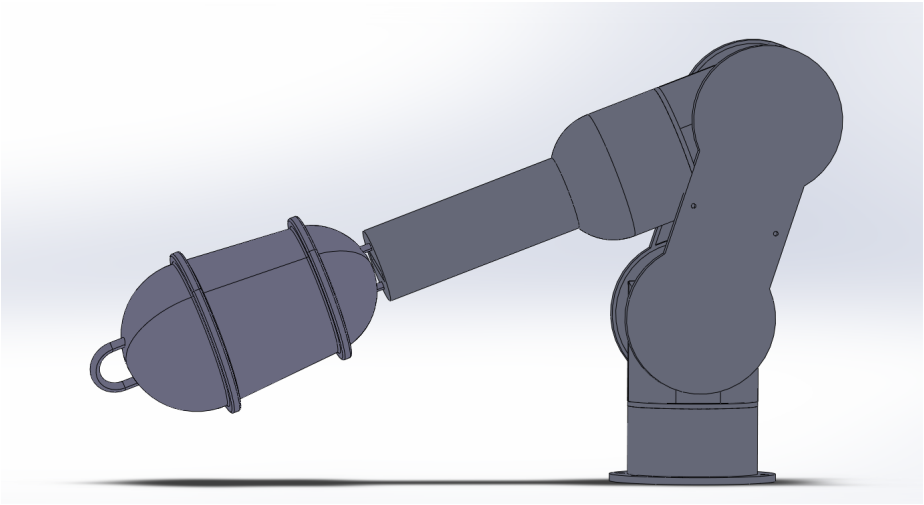

Figure 4.8: Rotary Joint Motion in Clockwise Direction

The rotary joint is crucial for power capture from the wave in the pitching mode of the buoy. The joint can be attached to a rotational electric generator to convert the buoy's pitching motion due to the waves in to electricity. The design is specific to achieve power capture in the pitch mode, whereas for the heaving mode a prismatic joint is explored in the following section.

The joint can also be used in the clockwise direction to pull the buoy out of the ocean if the wave environment gets harsh, for instance, in case of storms.

4.2.3 Prismatic Joint

A prismatic joint allows linear motion between a link, a base, and an end effector. The motion in this joint is constrained, meaning the joint has one DOF. A prismatic joint has a moving component called a slider which extends and retracts allowing linear electro-mechanical conversion. Figures 4.9 and 4.10 show the slider when the prismatic joint is extended and retracted, respectively. The slider also includes a slot to rigidly connect with

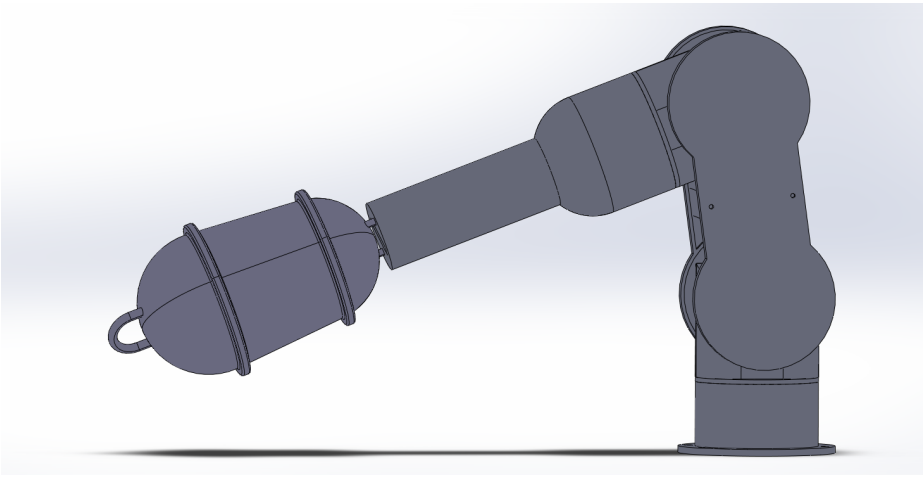

Figure 4.9: Prismatic joint when Extended

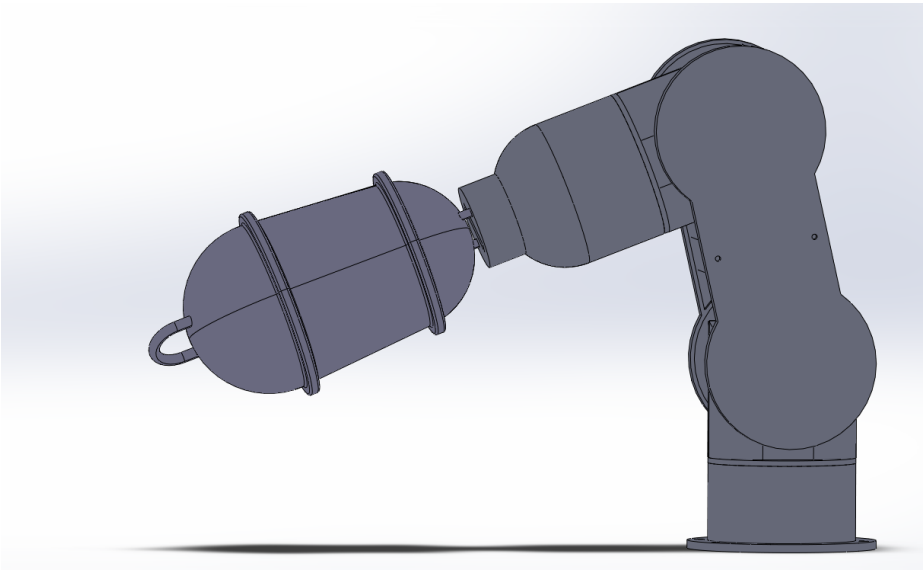

Figure 4.10: Prismatic joint when Retracted

the buoy as shown in Figure 4.11.

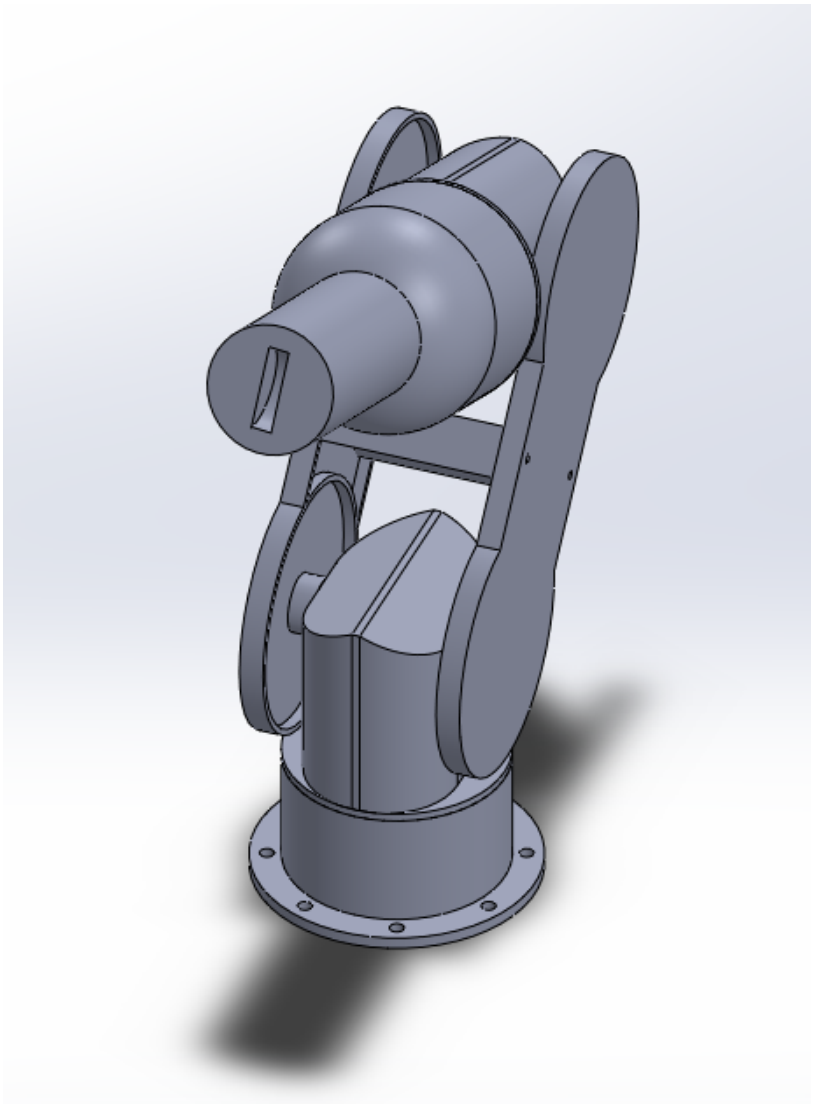

Figure 4.11: Buoy Connector Slot in the Slider of Prismatic Joint

This research requires power to be captured in the heaving motion of the buoy as well. In the heave mode, the buoy moves up and down and that linear motion can be translated to electricity by a linear generator attached to the prismatic joint. Therefore, the two joints (rotary and prismatic) are envisioned to operate independently being solely responsible for power capture in their respective DOF. The several views of the WEC assembly are enclosed in the Appendix: Figures A.8 - A.12, respectively.

WEC Material Selection

Although using a similar material as the buoy namely High density Polyethylene (HDPE) is possible, the robot's payload decreases significantly when using plastics. Also, the robot is not placed in the water but near-shore on a platform/dock, therefore, the robot can be made

of metal with a corrosion resistant coating that enables less maintenance and bio-fouling. Hence, a grade 304 – austenite stainless steel is used with an additional coat of chromium to increase corrosion resistance and durability in seawater environment. The selected material properties such as Young's Modulus, density, and other given material properties were used in the SolidWorks CAD environment to get the robot's properties tabulated in Table 4.2.

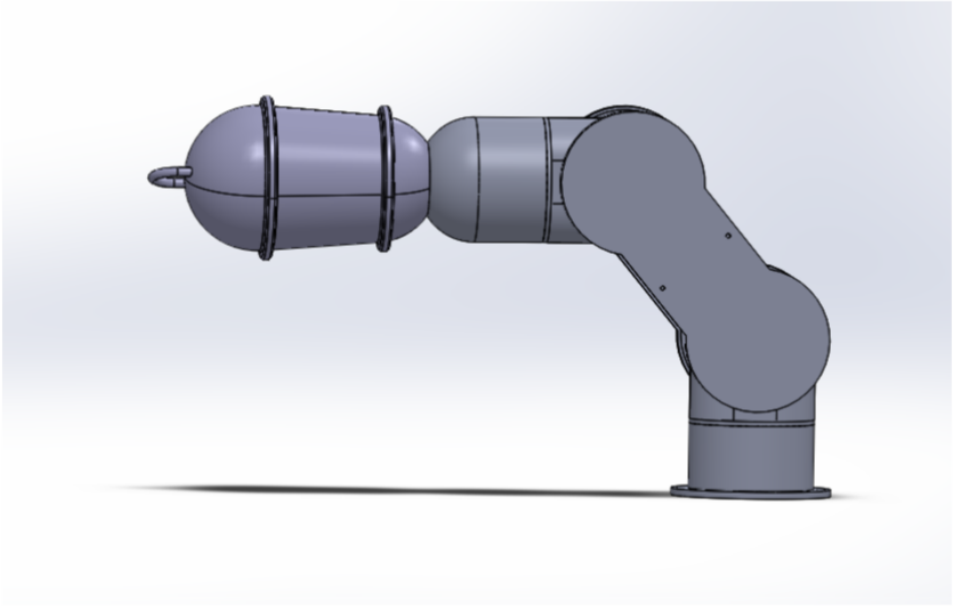

Figure 4.12: Wave Energy Converter Robotic Assembly – Fully Retracted Prismatic Joint Position

WEC Properties

The robot needs to be able to harness wave energy as well as host the buoy in the waves, hence the payload is massive. The robot's specifications are found in the following Table 4.2 and the robot assembly with the buoy is built in SolidWorks and shown in Figures 4.12 and 4.13. Figure 4.13 also shows the different materials used in the WEC assembly. The black representing 304 – Austenite stainless steel and orange denoting the use of High density Polyethylene (HDPE) for the buoy.

4.2.4 2 DOF Robot-WEC Model in Vector Form

The generalized coordinates correspond to the DOF of the robot, i.e., for revolute joints, the single DOF q_i corresponds to the rotation angle of the joint θ_i and in case of a prismatic joint, q_i represents the linear displacement d_i. In vector form, the generalized robot dynamics of a two-link planar robot are

Figure 4.13: Wave Energy Converter Robotic Assembly – Fully Extended Prismatic Joint Position

Characteristic Name	Value
Maximum reach	3202 mm
Rated payload	1300 kg
Maximum payload	1300 kg
Pose repeatability (ISO 9283)	+/− 0.1 mm
Number of axes	2
Weight approx.	4690 kg
Revolute joint angle (θ_1)	-130 deg
Mass of link 2 (m_2)	2350 kg
Length of link 2 (d_2)	1400 mm
Maximum force (F_R)	70,000 N
Robot torque (τ_{PTO})	99,700 Nm

Table 4.2: 2 Degrees-of-Freedom Robot Specifications

$$q = \begin{pmatrix} q_1 \\ q_2 \end{pmatrix} = \begin{pmatrix} \theta \\ d \end{pmatrix} \tag{4.2}$$

$$\dot{q} = \begin{pmatrix} \dot{q_1} \\ \dot{q_2} \end{pmatrix} = \begin{pmatrix} \dot{\theta} \\ \dot{d} \end{pmatrix} \tag{4.3}$$

$$\ddot{q} = \begin{pmatrix} \ddot{q_1} \\ \ddot{q_2} \end{pmatrix} = \begin{pmatrix} \ddot{\theta} \\ \ddot{d} \end{pmatrix} \tag{4.4}$$

$$M(q) = \begin{pmatrix} m_1 & 0 \\ 0 & m_2 \end{pmatrix} \tag{4.5}$$

$$I_r = \begin{pmatrix} I_{xi} & 0 & 0 \\ 0 & I_{yi} & 0 \\ 0 & 0 & I_{zi} \end{pmatrix} \tag{4.6}$$

where I_r is the inertia tensor of the robotic joints with mass m_i. For a 2 DOF robot, n=2, therefore, the Jacobian which provides the relation between the linear J_v, angular J_w joint velocities (q), and end-effector velocities (V) of a robot manipulator [78] is given by a 6×2 matrix as

$$J_R(q) = \begin{bmatrix} J_v \\ J_w \end{bmatrix}_{6Xn} = \begin{bmatrix} J_{11} & J_{12} \\ J_{21} & J_{22} \\ J_{31} & J_{32} \\ J_{41} & J_{42} \\ J_{51} & J_{52} \\ J_{61} & J_{62} \end{bmatrix} \tag{4.7}$$

The first three rows of the matrix indicate linear velocities of Joint 1 and 2 while the remaining rows describe the angular velocity of the same joints. In the figure 4.14, the links of the RP manipulator in this research are displayed and have the inertia tensors as follows

$$I_{r1} = \begin{bmatrix} I_{xx1} & 0 & 0 \\ 0 & I_{yy1} & 0 \\ 0 & 0 & I_{zz1} \end{bmatrix} \tag{4.8}$$

$$I_{r2} = \begin{bmatrix} I_{xx2} & 0 & 0 \\ 0 & I_{yy2} & 0 \\ 0 & 0 & I_{zz2} \end{bmatrix} \tag{4.9}$$

where I_{r1} and I_{r2} are the inertia tensor of the robotic joints 1 and 2 respectively. The total mass of the robot is m_1 and m_2 and, as illustrated in Figure 4.14, the center of mass of link 1 is located at a distance l_1 from the revolute joint 1 axis, the angle made by the revolute joint is measured as θ_1 and the center of mass of link 2 is at the variable distance d_2 from the revolute joint 1 axis. The equations of motion from Chapter 2 (equation 2.3- 2.19) are used in this section. It is noted that the equations in Chapter 2 are for 6 DOF WEC models. However, in this chapter we consider only a 2 DOF WEC system - the heave and pitch vectors. Hence, the following equations will have only 2 rows or columns in their matrices. Using Lagrangian dynamics and partial differentiation [79], the equations of motion (refer to equation 2.11) for this robotic manipulator are obtained as

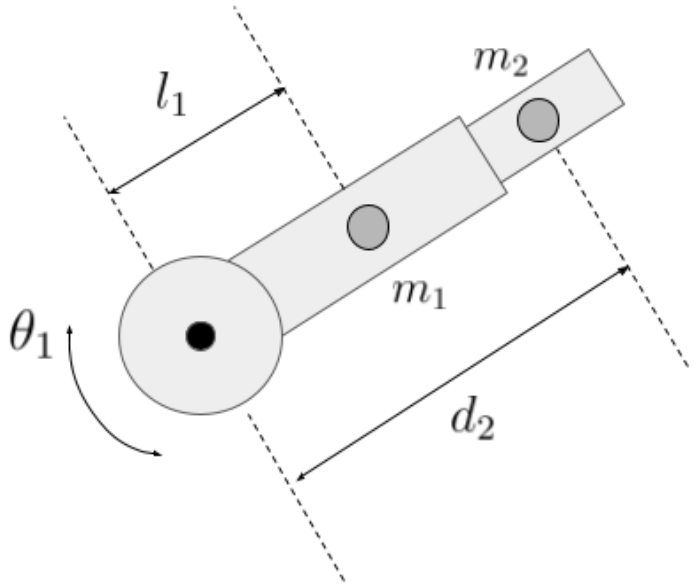

Figure 4.14: Dynamic Model of RP (Rotary-Prismatic) Manipulator

$$\begin{bmatrix} (m_1 l_1^2 + I_{zz1} + m_2 d_2^2 + I_{zz2}) & 0 \\ 0 & m_2 \end{bmatrix} \begin{bmatrix} \ddot{\theta_1} \\ \ddot{d_2} \end{bmatrix} + \begin{bmatrix} 2m_2 d_2 \dot{\theta_1} \dot{d_2} \\ -m_2 d_2 \dot{\theta_1}^2 \end{bmatrix} + \begin{bmatrix} (m_1 l_1 + m_2 d_2) g cos_{\theta_1} \\ m_2 g sin_{\theta_1} \end{bmatrix} = \begin{bmatrix} \tau_{PTO} \\ F_{PTO} \end{bmatrix} - J_R(q)^T \begin{bmatrix} \tau_r \\ F_r \end{bmatrix} \tag{4.10}$$

where

$$M(q) = \begin{bmatrix} (m_1 l_1^2 + I_{zz1} + m_2 d_2^2 + I_{zz2}) & 0 \\ 0 & m_2 \end{bmatrix} \tag{4.11}$$

$$V(q, \dot{q}) = \begin{bmatrix} 2m_2 d_2 \dot{\theta_1} \dot{d_2} \\ -m_2 d_2 \dot{\theta_1}^2 \end{bmatrix} \tag{4.12}$$

$$G(q) = \begin{bmatrix} (m_1 l_1 + m_2 d_2) g cos_{\theta_1} \\ m_2 g sin_{\theta_1} \end{bmatrix} \tag{4.13}$$

where F_r and τ_r are the robot forces acting on the prismatic and revolute joint respectively, τ_{PTO} is the moment force due to the revolute joint and F_{PTO} is the force due to the prismatic joint. The 2×2 matrix before the F_R, robot forces matrix is the $J_R(q)$ matrix, also known as the robot Jacobian referring to equation (4.7) is given by the following matrix.

$$J_R(q) = \begin{bmatrix} 0 & 0 \\ 0 & 0 \\ 0 & 1 \\ 0 & 0 \\ 0 & 0 \\ 1 & 0 \end{bmatrix} \tag{4.14}$$

Since the robot is solely exerting velocities in the z direction, the Jacobian is simplified as

$$J_R(q) = \begin{bmatrix} 0 & 1 \\ 1 & 0 \end{bmatrix} \tag{4.15}$$

The Jacobian's transpose is then calculated to be

$$J_R(q)^T = \begin{bmatrix} 0 & 1 \\ 1 & 0 \end{bmatrix} \tag{4.16}$$

Then, the equation of moment and force of the revolute and prismatic joint of the PTO system in vector form is given in the following equations respectively.

$$\tau_{PTO} - F_r = (m_1 l_1^2 + I_{zz1} + m_2 d_2^2 + I_{zz2})\ddot{\theta_1} + 2m_2 d_2 \dot{\theta_1} \dot{d_2} + (m_1 l_1 + m_2 d_2) g cos_{\theta_1} \tag{4.17}$$

$$F_{PTO} - \tau_r = m_2 \ddot{d_2} - m_2 d_2 \dot{\theta_1}^2 + m_2 g sin_{\theta_1} \tag{4.18}$$

The dynamic terms of the Cartesian form are necessary for the realization of overall WEC dynamics, hence, referring to equations (2.15-2.18), the following equations are obtained.

$$\begin{bmatrix} 0 & (m_1 l_1^2 + I_{zz1} + m_2 d_2^2 + I_{zz2}) \\ m_2 & 0 \end{bmatrix} \begin{bmatrix} \ddot{\theta_p} \\ \ddot{h} \end{bmatrix} + \begin{bmatrix} 2m_2 d_2 \dot{\theta_p} \dot{h} \\ -m_2 d_2 \dot{\theta_p}^2 \end{bmatrix} + \begin{bmatrix} (m_1 l_1 + m_2 d_2) g cos_{\theta_p} \\ m_2 g sin_{\theta_p} \end{bmatrix} = J_R(q)^{-T} \begin{bmatrix} \tau_{PTO} \\ F_{PTO} \end{bmatrix} - \begin{bmatrix} \tau_r \\ F_r \end{bmatrix} \tag{4.19}$$

where

$$M_x(q) = \begin{bmatrix} 0 & (m_1 l_1^2 + I_{zz1} + m_2 d_2^2 + I_{zz2}) \\ m_2 & 0 \end{bmatrix} \tag{4.20}$$

$$V_x(q, \dot{q}) = \begin{bmatrix} 2m_2 d_2 \dot{\theta_p} \dot{h} \\ -m_2 d_2 \dot{\theta_p}^2 \end{bmatrix} \tag{4.21}$$

$$G_x(q) = \begin{bmatrix} (m_1 l_1 + m_2 d_2) g cos_{\theta_p} \\ m_2 g sin_{\theta_p} \end{bmatrix} \tag{4.22}$$

$$J_R(q)^{-T} = \begin{bmatrix} 0 & 1 \\ 1 & 0 \end{bmatrix}^{-T} \tag{4.23}$$

$$\ddot{X} = \begin{bmatrix} \ddot{\theta_p} \\ \ddot{h} \end{bmatrix} \tag{4.24}$$

$$\dot{X} = \begin{bmatrix} \dot{\theta_p} \\ \dot{h} \end{bmatrix} \tag{4.25}$$

$$X = \begin{bmatrix} \theta_p \\ h \end{bmatrix} \tag{4.26}$$

The modes in the time-domain are h, the displacement of the buoy in heave and θ_p, the angular displacement of the buoy in pitch at time t. The buoy dynamics are therefore a function of the pitch motion (θ_p) and the heaving translation (h) of the buoy due to the ocean waves. Then, the equation of moment and force of the revolute and prismatic joint of the PTO system in vector Cartesian form is calculated respectively as

$$F_{PTO} - \tau_r = (m_1 l_1^2 + I_{zz1} + m_2 d_2^2 + I_{zz2})\ddot{h} + 2m_2 d_2 \dot{\theta_p} \dot{h} + (m_1 l_1 + m_2 d_2) g cos_{\theta_p} \tag{4.27}$$

$$\tau_{PTO} - F_r = m_2 \ddot{\theta_p} - m_2 d_2 \dot{\theta_p^2} + m_2 g sin_{\theta_p} \tag{4.28}$$

The WEC system also considers the wave-buoy interaction, hence expanding equation (2.3) in matrix form as

$$\begin{bmatrix} (I_{r0} + a_{55}) & (z_G.m + a_{53}) \\ (z_G.m + a_{35}) & (m + a_{33}) \end{bmatrix} \begin{bmatrix} \ddot{\theta_p} \\ \ddot{h} \end{bmatrix} + \begin{bmatrix} b_{55} & b_{53} \\ b_{35} & b_{33} \end{bmatrix} \begin{bmatrix} \dot{\theta_p} \\ \dot{h} \end{bmatrix} + \begin{bmatrix} c_{55} & c_{53} \\ c_{35} & c_{33} \end{bmatrix} \begin{bmatrix} \theta_p \\ h \end{bmatrix} = \begin{bmatrix} \tau_r \\ F_r \end{bmatrix} + \begin{bmatrix} \tau_{e5} \\ F_{e3} \end{bmatrix} \tag{4.29}$$

$$[M + A_h] = \begin{bmatrix} (I_{r0} + a_{55}) & (z_G.m + a_{53}) \\ (z_G.m + a_{35}) & (m + a_{33}) \end{bmatrix} \tag{4.30}$$

$$B = \begin{bmatrix} b_{55} & b_{53} \\ b_{35} & b_{33} \end{bmatrix} \tag{4.31}$$

$$C = \begin{bmatrix} c_{55} & c_{53} \\ c_{35} & c_{33} \end{bmatrix} \tag{4.32}$$

$$F_e(t) = \begin{bmatrix} \tau_{e5} \\ F_{e3} \end{bmatrix} \tag{4.33}$$

$$F_R(t) = \begin{bmatrix} \tau_r \\ F_r \end{bmatrix} \tag{4.34}$$

where z_G is the coordinates of the center of gravity of the buoy on the vertical axis, M is the dry mass of the buoy and I_r0 is the moment of inertia of the buoy in pitch. The added mass, hydrostatic restoring and radiation damping coefficients are represented by a_{ij}, $c_{i,j}$ and b_{ij} where $i, j = 5, 3$ represents pitch and heave modes respectively.The τ_{e5} term represents the moment of the wave excitation in pitch. The combination of equations (4.29) and (4.19) give us the dynamics of WEC system as

$$M_x(q)\begin{bmatrix}\ddot{\theta_p}\\ \ddot{h}\end{bmatrix} + V_x(q,\dot{q}) + G_x(q) = J_R(q)^{-T}\begin{bmatrix}\tau_{PTO}\\ F_{PTO}\end{bmatrix} - \begin{bmatrix}\tau_r\\ F_r\end{bmatrix} \tag{4.35}$$

$$\begin{aligned}\begin{bmatrix}\tau_r\\ F_r\end{bmatrix} = \begin{bmatrix}(I_{r0}+a_{55}) & (z_G.m+a_{53})\\ (z_G.m+a_{35}) & (m+a_{33})\end{bmatrix}\begin{bmatrix}\ddot{\theta_p}\\ \ddot{h}\end{bmatrix} + \begin{bmatrix}b_{55} & b_{53}\\ b_{35} & b_{33}\end{bmatrix}\begin{bmatrix}\dot{\theta_p}\\ \dot{h}\end{bmatrix}\\ + \begin{bmatrix}c_{55} & c_{53}\\ c_{35} & c_{33}\end{bmatrix}\begin{bmatrix}\theta_p\\ h\end{bmatrix} - \begin{bmatrix}\tau_{e5}\\ F_{e3}\end{bmatrix}\end{aligned} \tag{4.36}$$

$$\begin{aligned}WEC_{mass}\begin{bmatrix}\ddot{\theta_p}\\ \ddot{h}\end{bmatrix} = \begin{bmatrix}0 & 1\\ 1 & 0\end{bmatrix}^{-T}\begin{bmatrix}\tau_{PTO}\\ F_{PTO}\end{bmatrix} - (V_x(q,\dot{q}) + G_x(q) + B\begin{bmatrix}\dot{\theta_p}\\ \dot{h}\end{bmatrix}\\ + C\begin{bmatrix}\theta_p\\ h\end{bmatrix} - \begin{bmatrix}\tau_{e5}\\ F_{e3}\end{bmatrix})\end{aligned} \tag{4.37}$$

$$WEC_{mass} = \begin{bmatrix}I_{r0}+a_{55} & (m_1l_1^2 + I_{zz1} + m_2d_2^2 + I_{zz2} + (z_G.m + a_{53}))\\ (m_2 + z_G.m + a_{35}) & (m+a_{33})\end{bmatrix} \tag{4.38}$$

In vector form equation (4.37) is written as follows for pitch and heave mode respectively

$$\begin{aligned}(I_{r0}+a_{55})\ddot{\theta_p} + m_p\ddot{h} = F_{PTO} - [2m_2d_2\dot{\theta_p}\dot{h} + (m_1l_1 + m_2d_2)gcos_{\theta_p}\\ + b_{53}\dot{h} + b_{55}\dot{\theta_p} + (c_{55}.r_G^2)\theta_p - \tau_{e5}]\end{aligned} \tag{4.39}$$

$$m_p = (m_1l_1^2 + I_{zz1} + m_2d_2^2 + I_{zz2} + z_G.m + a_{53}) \tag{4.40}$$

$$\begin{aligned}(m_2 + z_G.m + a_{35})\ddot{\theta_p} + (m+a_{33})\ddot{h} = \tau_{PTO} - [-m_2d_2\dot{\theta_p}^2 + m_2gsin_{\theta_p}\\ + b_{33}\dot{h} + b_{35}\dot{\theta_p} + c_{33} - F_{e3}]\end{aligned} \tag{4.41}$$

If only the pitch motion of buoy displacement is considered, the system becomes 1 DOF and equation (4.39) is expressed as

$$(I_{r0}+a_{55})\ddot{\theta_p} = F_{PTO} - (m_1l_1 + m_2d_2)gcos_{\theta_p} - b_{55}\dot{\theta_p} - (c_{55}.r_G^2)\theta_p + \tau_{e5} \tag{4.42}$$

Similarly if the motion of the displacement of buoy is considered in heave mode, the equation (4.41) is given as follows

$$(m+a_{33})\ddot{h} = \tau_{PTO} - b_{33}\dot{h} - c_{33} + F_{e3} \tag{4.43}$$

4.3 Controller Design

4.3.1 Application of the Latching Strategy

The latching control force equation (3.35) is introduced in the WEC's dynamic motion equation (3.5):

$$[M_x(q) + M + A_h]\ddot{X} + B\dot{X} + CX = -Gl\dot{X} + F_e(t) \tag{4.44}$$

$$[M_x(q) + M + A_h]\ddot{X} + (B + Gl)\dot{X} + CX = F_e(t) \tag{4.45}$$

Then, rearranging the equation in terms of $\ddot{X}$ gives

$$\ddot{X} = [F_e(t) - (B + Gl)\dot{X} - CX][M_x(q) + M + A_h]^{-1} \tag{4.46}$$

Similarly, the equation in terms of $\dot{X}$ would be

$$\dot{X} = [F_e(t) - [M_x(q) + M + A_h]\ddot{X} - CX][(B + Gl)]^{-1} \tag{4.47}$$

The goal is to maximize the energy absorption over a duration T. Mathematically, it can be written as in the latching control paper as

$$max_l E(l) = \int_0^T B\dot{X}^2\, dt \tag{4.48}$$

Now, defining the Hamiltonian H according to equation (3.38):

$$H = B\dot{X}^2 + \lambda_1\dot{X} + \lambda_2([F_e(t) - (B + Gl)\dot{X} - CX][M_x(q) + M + A_h]^{-1}) \tag{4.49}$$

From equation (3.39), the adjoint state equations for this problem are given by:

$$\dot{\lambda_1} = C\lambda_2 \tag{4.50}$$

$$\dot{\lambda_2} = -2B\dot{X} - \lambda_1 + \lambda_2(B + Gl) \tag{4.51}$$

The Hamiltonian being a linear function of the control variable l, results in a latching control known as "bang- bang". This means that in order to maximize H, l has to be equal to values 0 or 1. Looking at equation (4.49), we see that, at each time, the Hamiltonian will be maximum if:

- l =1, when $(-\lambda_2 G\dot{X}) > 0$
- l = 0, otherwise.

Using equations (4.46), (4.47), (4.50), (4.51), and the above conditions, the latching control sequence l(t) can be derived for the WEC operating within the time interval [0, T]. The

average power absorbed is expressed as

$$P_{avg} = \lim_{T \to \infty} \frac{\int_0^T B\dot{X}^2 \, dt}{T} \tag{4.52}$$

The computation of the latching control law uses the iterative method described in the previous chapter. The incident wave is a multi-frequency regular waveform whose period is equal to 12 s and whose height is 2.5 m. The (large) damping coefficient G was set to $(G = 80([M_x(q) + M + A_h]))$, which happens to be the practical limit of this latching approach [61].

The controller parameters highlighted in Table 4.3, are used to get the simulation results which are compared with the results of the controller presented in the next chapter.

Controller Parameter	Value
(Large) Damping Coefficient (G)	$80([M_x(q) + M + A_h])$

Table 4.3: Latching Controller Parameters

4.3.2 Proposed Controller

The sliding mode extremum seeking controller as mentioned in the previous chapter, operates by having the performance function P_{avg} follow an increasing function of time g(t), irrespective of the unknown gradient $dP_{avg}/d\dot{X}$. This controller is applicable in practice due to the following reasons:

- The SM-ES control algorithm is a model-free approach.
- For the additional terms of the controller, the two hyperparameters K and ϵ, and ρ need to satisfy the following conditions to be viable:
    1. ρ, K and ϵ need to be greater than 0.
    2. To maintain stability of the overall system, the variation of the parameter u of the switching function needs to be much slower than the dynamics of the system. Therefore, the hyperparameters K and ϵ need to be significantly smaller than ρ.

The tuning of the gain parameters of the SM-ES controller was based on the trial and error method. The gains were tuned primarily based on the average power output reaching steady-state. The controller parameters used in the Simulation studies are highlighted in Table 4.4.

4.4 Conclusion

In this chapter, an introduction to the simulation parameters is provided. The deployment location selection process is highlighted and followed by the design of the buoy to extract

Controller Parameter	Value
K_σ (Pitch and Heave)	5
K_B (Pitch)	0.6
K_B (Heave)	0.8
K_C (Pitch)	0.1
K_C (Heave)	0.2
K (Pitch and Heave)	0.5
ρ (Pitch and Heave)	10
ϵ (Pitch and Heave)	0.1

Table 4.4: Proposed Controller Parameters

maximum power from the incident wave. The next part of the chapter dives into the design and modeling of a 2 DOF open kinematic chain WEC that is connected rigidly to the buoy and based near-shore. Then, the open kinematic chain robotic system design details are mentioned and the WEC properties highlighted for simulation study. The last part of this chapter introduces the two controllers used to study and compare the interaction between the sea state and the average power absorbed due to the combined effects of the 2 DOF WEC and floating buoy. The proposed controller and latching controller parameters are highlighted in this chapter. The simulation results in the following chapter are based on the case study parameters of this chapter.

Chapter 5

Simulation Results

In the following two sections, results from numerical simulations of the WEC using WEC-Sim are presented, followed by the proposed SM-ES control scheme as well as the latching controller performance.

5.1 Introduction to WEC-SIM

WEC-Sim is an acronym for Wave Energy Converter Simulator developed by Sandia National Laboratories and the National Renewable Energy Laboratory with assistance from the US Department of Energy. This is an open source code developed on the MATLAB-Simulink environment that solves the time-domain equations for rigid body motion based on the Cummins formulation. It also simulates the dynamics of a wave energy converter operating in the ocean waves.

WEC-Sim has the ability to model devices that are composed of rigid bodies, power take-off systems, and mooring systems [80]. It implements hydrodynamic coefficients derived from boundary element simulations in the frequency-domain, to model the relevant WEC-wave interaction, equation 2.1. The time-domain simulations in WEC-Sim are performed by numerical integration of the WEC equations of motion in 6 degrees-of-freedom [81]. The workflow for WEC-Sim is charted in Figure 5.1.

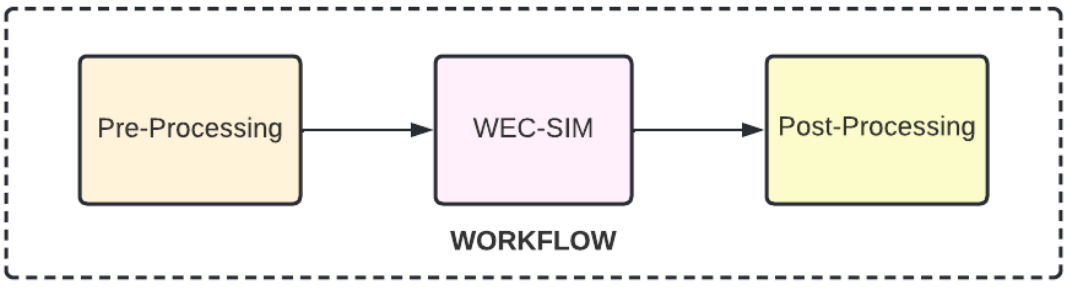

Figure 5.1: Block Diagram of the Wave Energy Converter Simulator Workflow

The pre-processing involves setting up the CAD Model, specifying WEC geometries and inertia-mass properties. The CAD file is generated from SolidWorks as a .stl file for this purpose. This process is followed by the WEC-Sim code generation step that involves designing a SIMULINK model and setting up the ocean environment with specifications such as wave conditions, simulation parameters, PTO constraints and body properties to simulate the sea-state. Once the WEC-Sim code is run, the post-processing step involves analyzing the results that generally include graphs of WEC device motion.

5.1.1 WEC-Sim Modeling

Hydrodynamic coefficients that describe radiation damping, wave diffraction force, and wave excitation force/ moment are widely used in multi-body dynamics simulations of wave energy converters, ships, offshore platforms, and other floating structures. The WEC-Sim modeling process flowchart is illustrated in Figure A.3 of the Appendix.

WEC-Sim simulation includes the rendering of the SolidWorks (.stl) files and the generation of the boundary element (.h5) files by BEMIO. The rendering of the CAD file into the WEC-Sim workspace is called the wave device specification step. This step is then followed by the numerical method step in which the time-domain dynamic response of the system is found by integrating the WEC system's equations of motion [82]. The WEC-Sim code uses the significant wave height (Hs) and peak period (Tp) of 2.5 meters and 12 seconds respectively. The code is used to generate regular waves and to provide the heave forces and pitch moments acting on the buoy.

5.1.2 WEC-Sim Results

The results from the WEC-Sim software are depicted in Figures 5.2 and 5.3. The pitch moments acting on the buoy with respect to time are plotted in the Figure 5.2. Similarly, in Figure 5.3 the heave forces acting on the buoy with respect to time is graphed. The buoy's forces/moments in both degrees-of-freedom are shown in the time-domain.

5.2 Controller Simulation Results

For evaluating the performance of the proposed SM-ES control based WEC system, simulation studies were conducted, and the results are demonstrated. The control systems were designed and evaluated using MATLAB-Simulink software.

The graphs (see Figures (5.4-5.9)) include three plots which are plotted against time with respect to buoy velocity and wave excitation force (heave) or moment (pitch), power output and average power respectively. The graphs are plotted for the 2 DOF system in heaving and pitching mode. The first two figures are the WEC system performance based on the latching controller whereas the last two figures depict the performance results based on the proposed SM-ES controller with the energy maximizing-desired speed function.

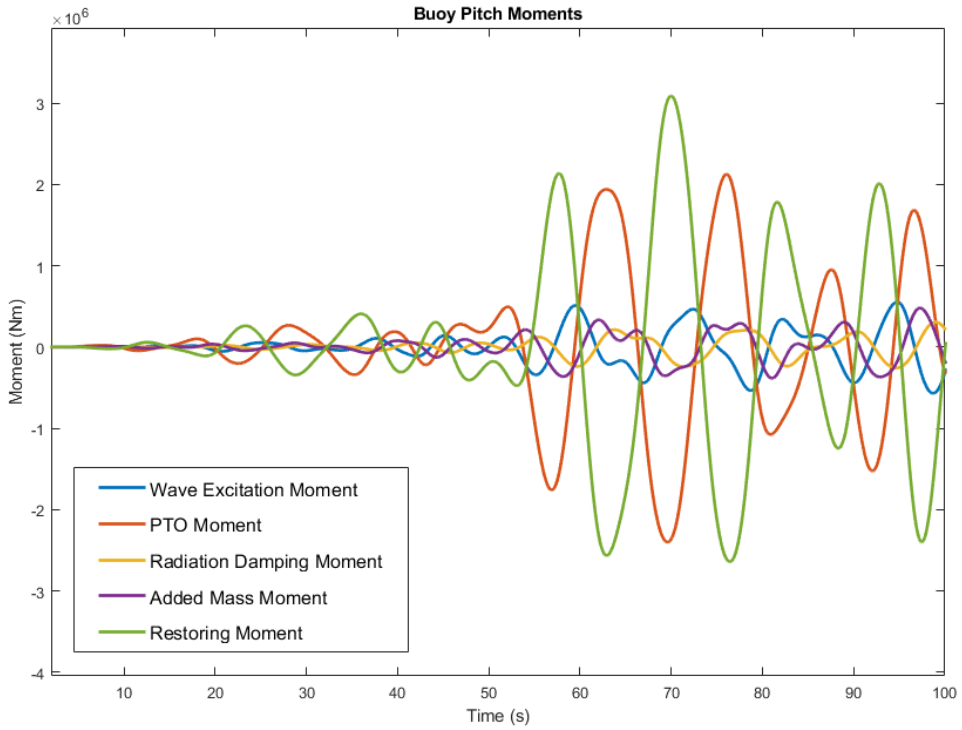

Figure 5.2: Wave Energy Converter Simulator Results: Moments acting on the Buoy in Pitch Motion

At first glance, when compared to the latching controller results in Figures (5.4-5.5), the proposed controller tracks more output power over time (see Figures (5.8-5.9)). This is specifically indicated in the average power extraction plot (dark brown/ maroon curve), where the SM-ES method results in a higher value. However, we observe from Appendix Figures A.4 - A.7, that the proposed controller takes longer than the latching controller to absorb more average power. This is likely due to the trial and error method of tuning the proposed controller. Also, the average power absorbed by the system is approximately 10^{-2} times the instantaneous power. This is most likely due to the estimation of the performance function depicted in Figure 3.3 and the total duration of simulation of each controller respectively.

To achieve maximum power absorption, the WEC system velocity and excitation force/ moment need to be in phase. The WEC system velocity is kept in phase with the excitation force/ moment by the SM-ES controller. This is depicted in the second plot of Figures (5.8-5.9) that have a blue curve indicating the wave excitation force/ moment and a purple curve indicating the buoy's velocity.

Figure 5.4 shows the WEC performance using latching control in heave motion. The first graph with the title "Latching Control - Velocity Tracking (Heave)" shows when the system

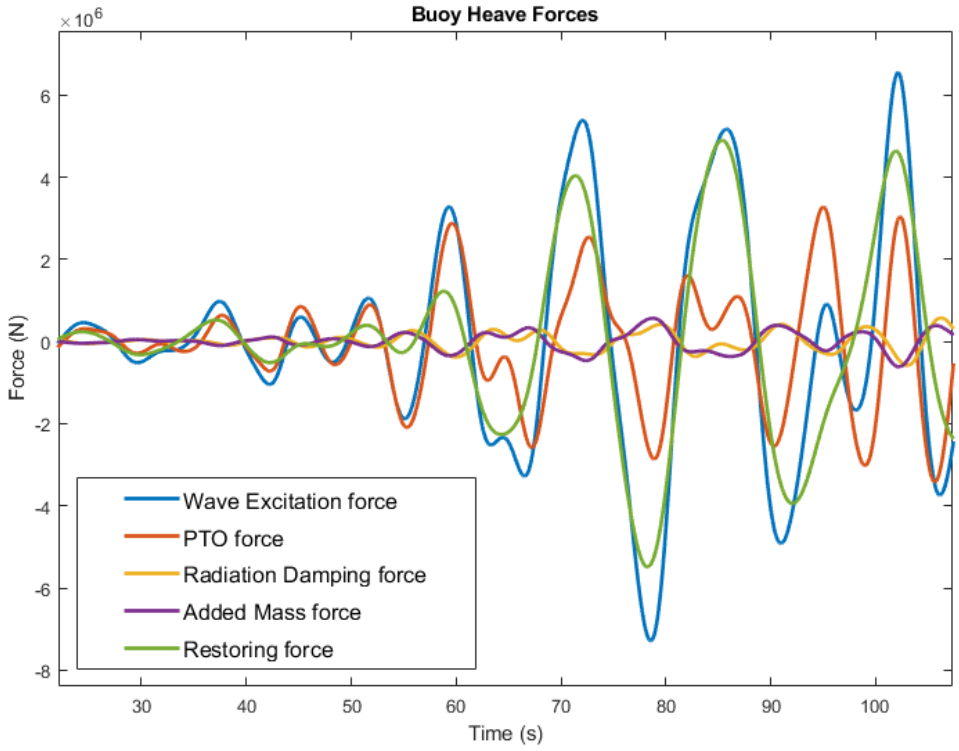

Figure 5.3: Wave Energy Converter Simulator Results: Forces acting on the Buoy in Heave Motion

is latched and unlatched. The latching duration is speculated to be very small, less than 5 seconds. This is likely due to the weaker model of latching control used. The second graph in the figure with the title "Latching Control - Actual Output of the WEC System (Heave)" shows the power absorbed by the WEC system while the last plot with the title "Latching Control - Average Power Output of the WEC system (Heave)" indicates the average power absorbed by the WEC system. The power absorbed by the WEC system (green curve) seems to indicate that power is absorbed even during latched seconds (i.e. when velocity is zero). But this is due to the resolution of the plot which when observed carefully, shows a slight step indicating some power is absorbed even in the latched state. The simulation results using the latching controller in heave motion from time 0s to 100s is enclosed in the Appendix Figure A.4 of this thesis.

Figure 5.5 depicts the WEC performance using latching control in pitch motion. The system when latched and unlatched is observed from the first graph with the title "Latching Control - Velocity Tracking (Pitch)". Since the latching duration is less than one second, it is very short. Most likely, this is a result of the weaker latching control model as mentioned above. The power absorbed by the WEC system is plotted against time in the second graph with the title "Latching Control - Actual Output of the WEC System (Pitch)". It appears

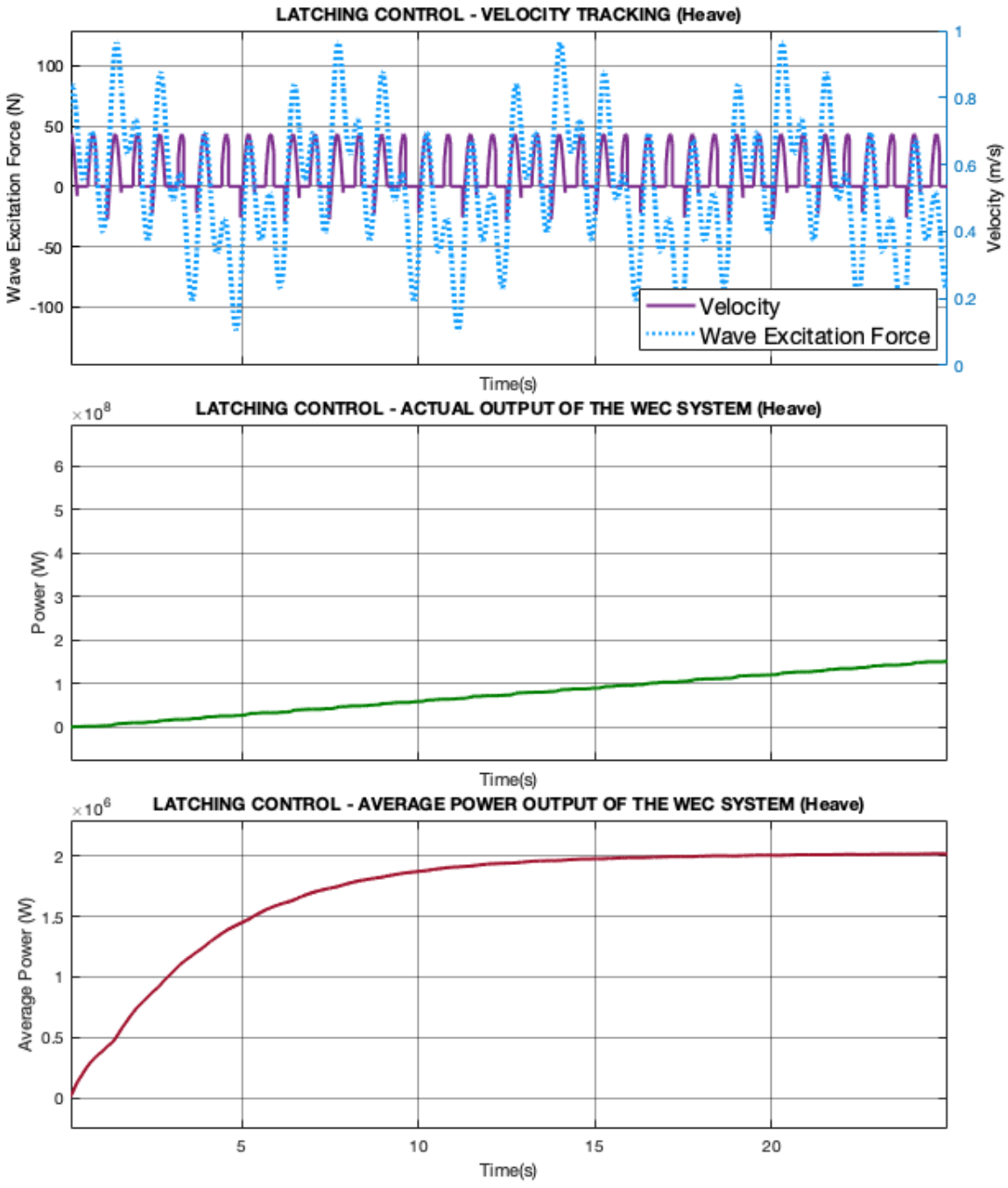

Figure 5.4: Simulation results: Latching control applied to the Wave Energy Converter Robotic System in Heave motion

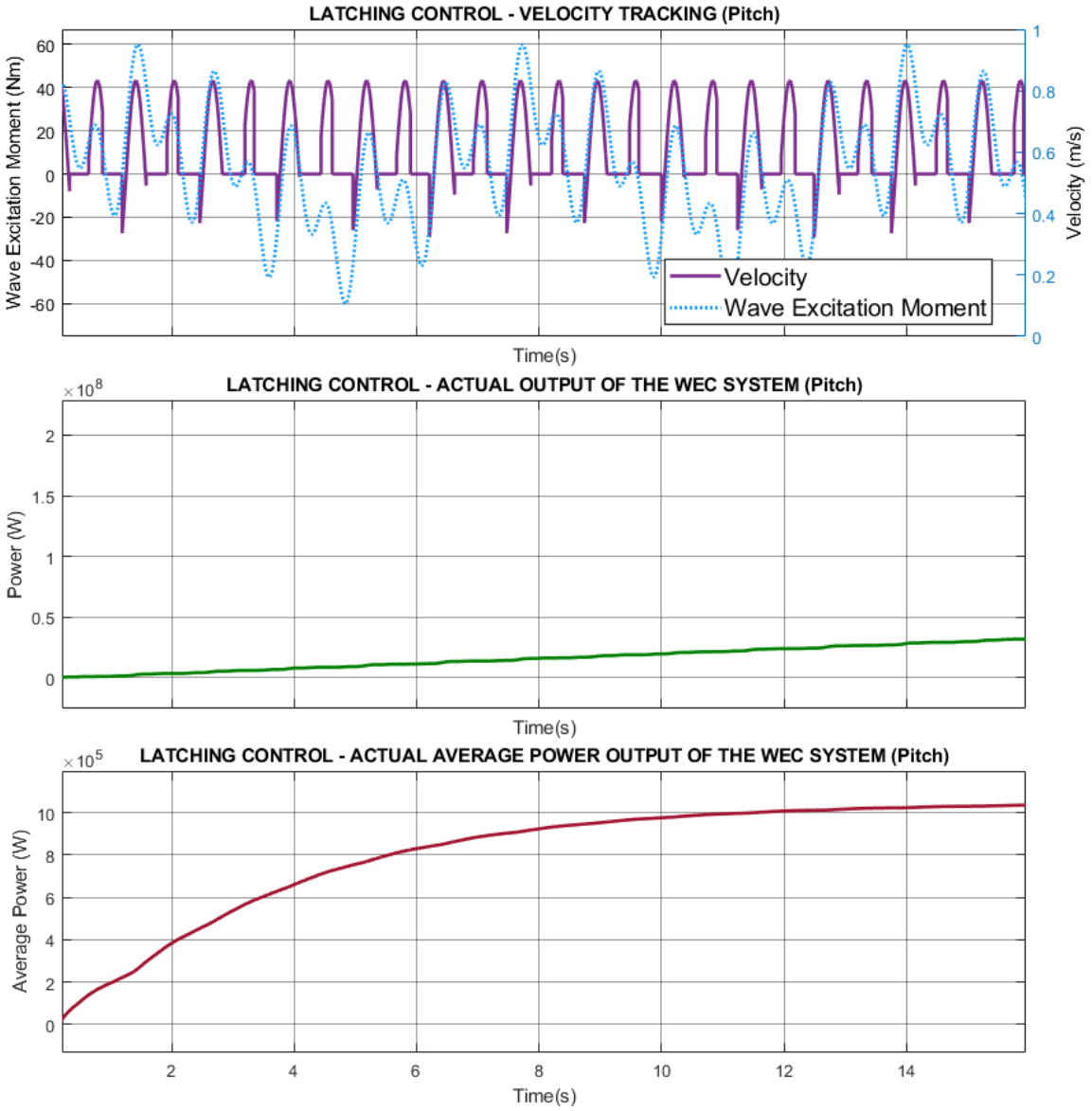

Figure 5.5: Simulation results: Latching control applied to the Wave Energy Converter Robotic System in Pitch motion

that the WEC system absorbs power (green curve) even during latched seconds (i.e. when velocity is zero). This is due to the plot resolution. Upon closer examination, there's a slight step indicating that there is some power absorbed even during the latched state. The final plot in the figure with the title "Latching Control - Average Power Output of the WEC system (Pitch)" shows the average power absorbed by the WEC system. Starting at 12 seconds, we can observe that the latching controller absorbs steady average power. The Appendix Figure A.5 of this thesis contains simulation results using latching controller in pitch motion from time 0s to 100s.

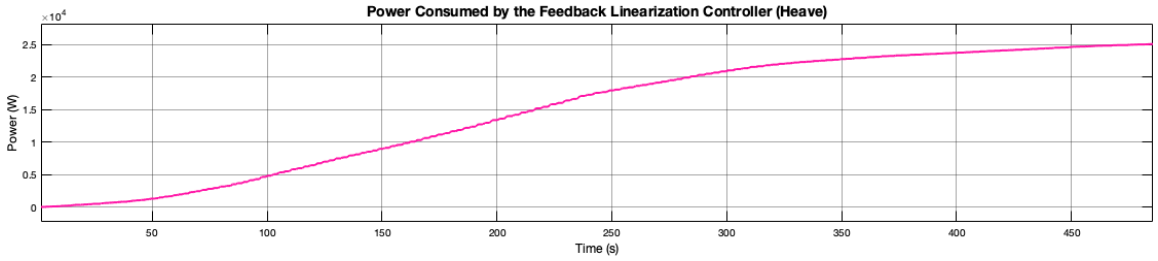

Figure 5.6: Power Consumed by the Feedback Linearization Controller in Heave motion

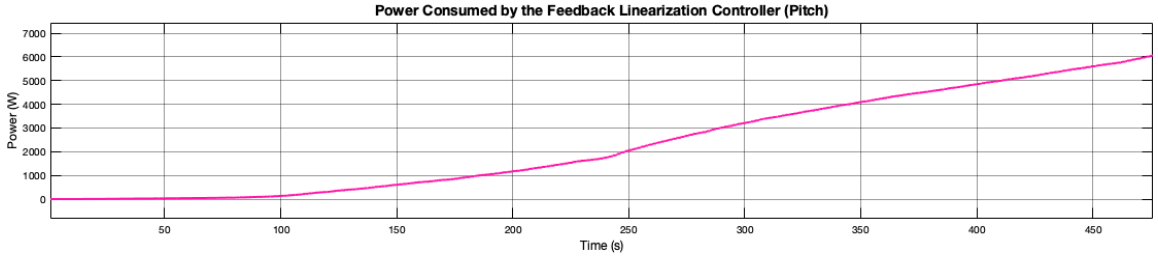

Figure 5.7: Power Consumed by the Feedback Linearization Controller in Pitch motion

Before analyzing the proposed controller results, we observe the power consumption during linearization of the non-linear WEC system as mentioned in equation (3.3). The power consumed by the feedback linearization controller is 2.5 X 10^4 W (in heave) and is 6 X 10^3 W (in pitch), as depicted in Figure 5.6 and Figure 5.7 respectively. The power consumed by the feedback linearizing controller is compared later in this section with the power absorbed by the SM-ES controller.

The WEC performance using the proposed SM-ES control in heave motion is shown in Figure 5.8. The first graph with the title "Velocity Tracking (Heave)" shows when the buoy's velocity follows the wave excitation force. The second graph in the figure with the title "Actual Output of the WEC System (Heave)" shows the power absorbed by the WEC system while the last plot with the title "Average Power Output of the WEC system (Heave)" indicates the average power absorbed by the WEC system. The simulation results using the SM-ES controller in heave motion from time 0s to 140s is enclosed in the Appendix Figure A.6 of this thesis. From figure A.6, the delay in reaching steady average power absorption

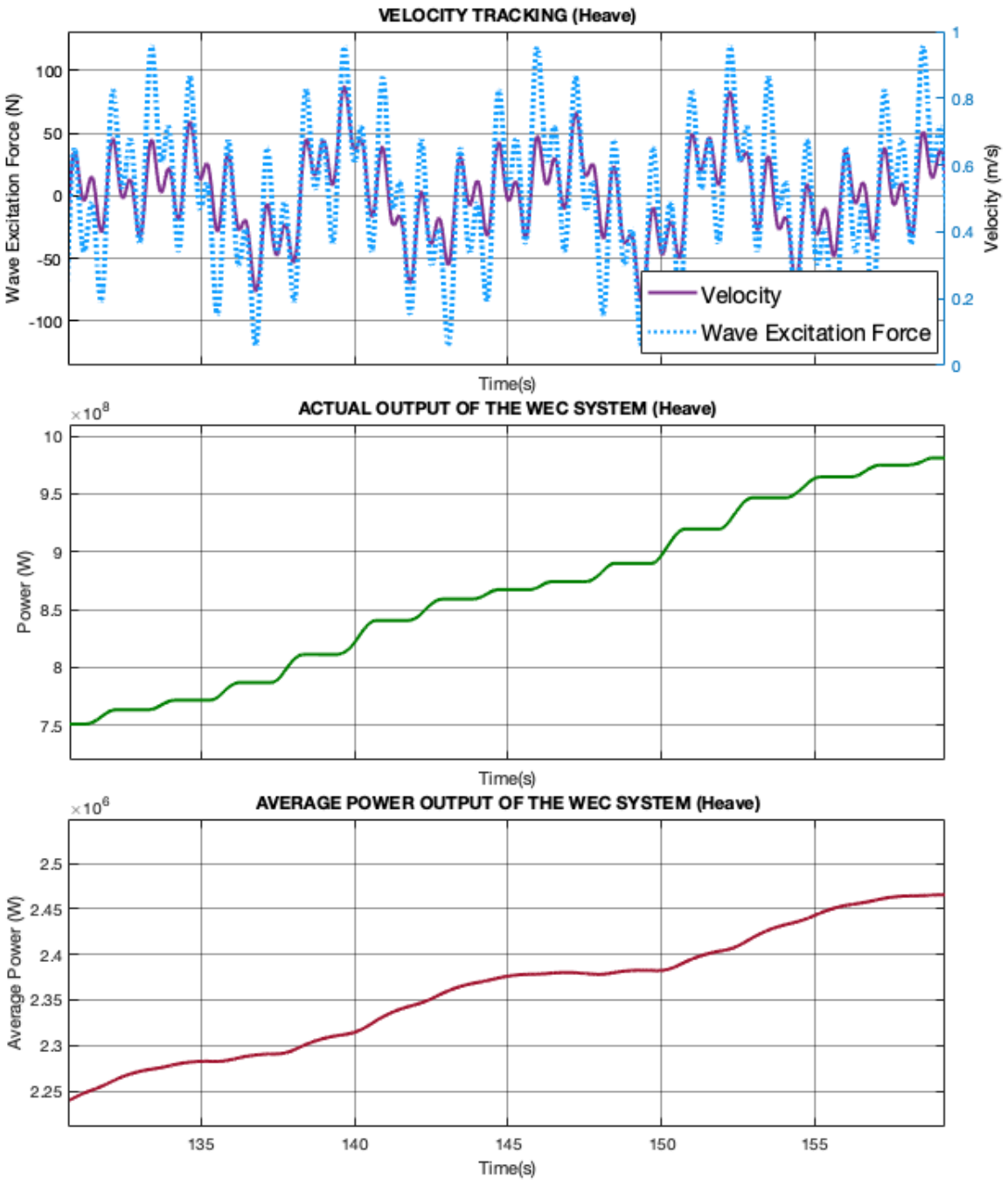

Figure 5.8: Simulation results: Proposed Sliding Mode Extremum Seeking Control applied to the Wave Energy Converter Robotic System in Heave motion

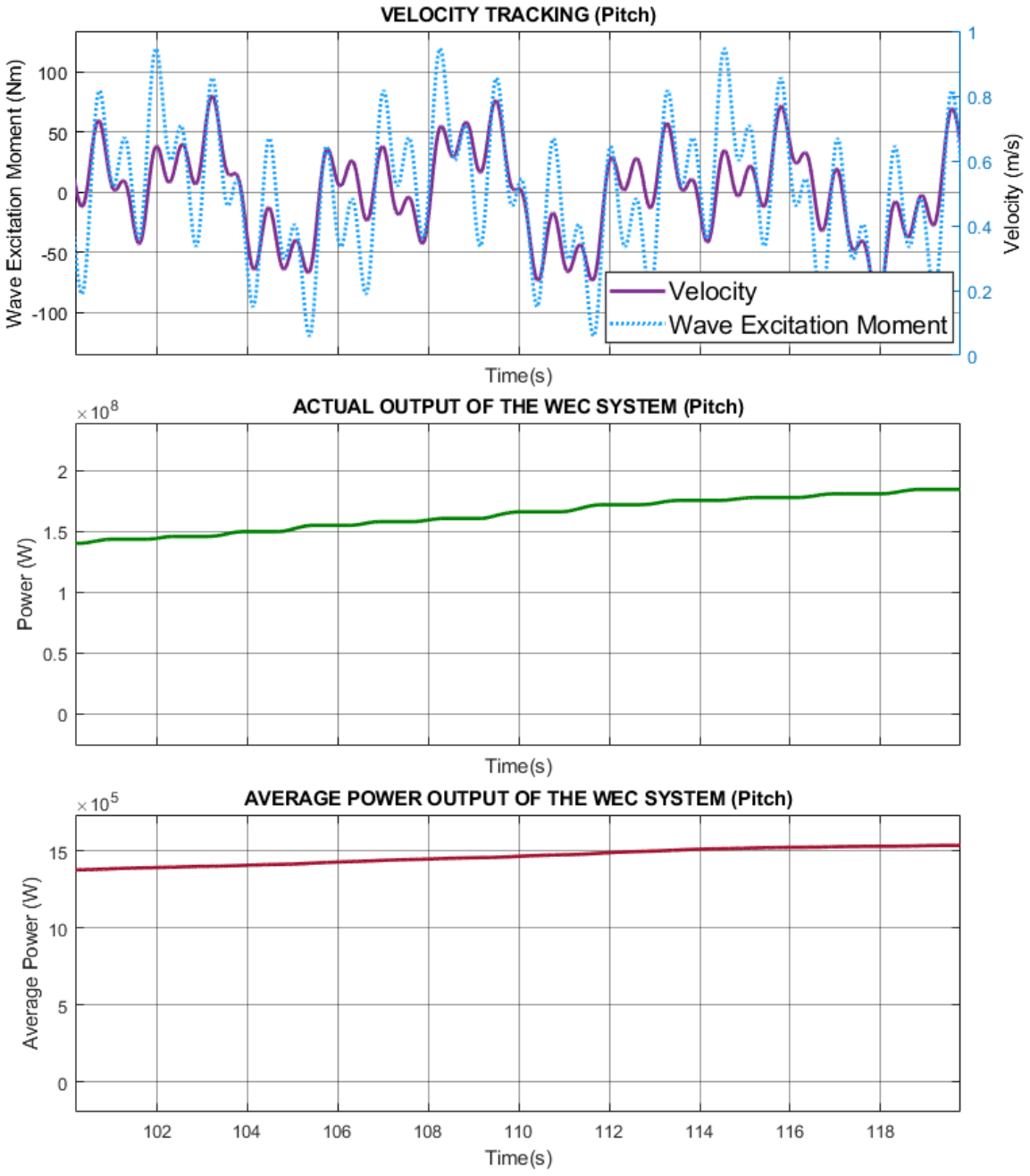

Figure 5.9: Simulation results: Proposed Sliding Mode Extremum Seeking Control applied to the Wave Energy Converter Robotic System in Pitch motion

Proposed Controller (DOF)	Power
Feedback Linearization Controller (Heave)	2.5 X 10^4 W
Feedback Linearization Controller (Pitch)	6 X 10^3 W
SM-ES Controller (Heave)	9.75 $\times$ 10^8 W
SM-ES Controller (Pitch)	1.8 $\times$ 10^8 W

Table 5.1: Results of the Power Absorbed by SM-ES controller and the Power Consumed by Feedback Linearization controller in Pitch and Heave Motion

Controller (DOF)	Average Power Absorbed
Latching Controller (Heave)	2.03 $\times$ 10^6 W
Latching Controller (Pitch)	10.2 $\times$ 10^5 W
SM-ES Controller (Heave)	2.25 $\times$ 10^6 W
SM-ES Controller (Pitch)	15.6 $\times$ 10^5 W

Table 5.2: Results of the Average Power Absorbed by SM-ES and Latching controller in Pitch and Heave Motion

is postulated to be due to the trial and error control parameter tuning strategy. Future research can be conducted to improve the proposed controller's convergence rate which may enhance the power absorption as well.

Figure 5.9 depicts the performance of the WEC system using the proposed SM-ES control in pitch motion. As shown in the graph with the title "Velocity Tracking (Pitch)," the buoy's velocity follows the wave excitation moment. In the figure, the second graph with the title "Actual Output of the WEC System (Pitch)" shows the power absorbed by the WEC system while the last plot with the title "Average Power Output of the WEC system (Pitch)" shows the average power absorbed.The Appendix Figure A.7 of this thesis contains simulation results using the SM-ES controller in pitch motion from time 0s to 140s. As a result of trial and error control parameter tuning, it is speculated from Figure A.7 that steady average power absorption takes longer than expected as mentioned above.

The power lost during feedback linearization of the system is tabulated along with power absorption of the system in Table 5.1. It can be observed that the instantaneous power absorbed by the system is 39 X 10^3 times more than the power lost during feedback linearization in the heave motion. Similarly, we observe the instantaneous power absorbed by the system in pitch motion is 30 X 10^3 times more than the power lost during linearization of the non-linear WEC system. Overall, we observe that the power loss during feedback linearization of the system is significantly less than the overall power absorbed by the system. The energy consumed is speculated to be relatively less due to the additional force provided by the robot and the buoyancy force. These forces compensate and linearize the reaction forces present due to gravity, centrifugal and Coriolis effects. Thereby, resulting in the feedback linearization controller consuming relatively negligible energy to linearize the WEC system.

From Table 5.2, it is seen that the latching controller enables the WEC system to harness average power of approximately 2.03 $\times$ 10^6 W (heave) in 15 seconds and 10.2 $\times$ 10^5 W (pitch) in 20 seconds. Whereas the proposed controller can harness average power of about 2.25 $\times$ 10^6 W (heave) in 120 seconds and 15.6 $\times$ 10^5 W (pitch) in 115 seconds. The proposed controller's average power output is 1.1 times the latching controller's output during heave motion after 120 seconds. Similarly, we can see that the average power output of the SM-ES controller is 1.5 times the latching controller during pitch motion after 115 seconds. In this case study, the proposed controller absorbs more average power compared to the latching controller overtime. However, the proposed controller takes significantly longer with respect to the latching controller to reach a comparable average power absorption state.

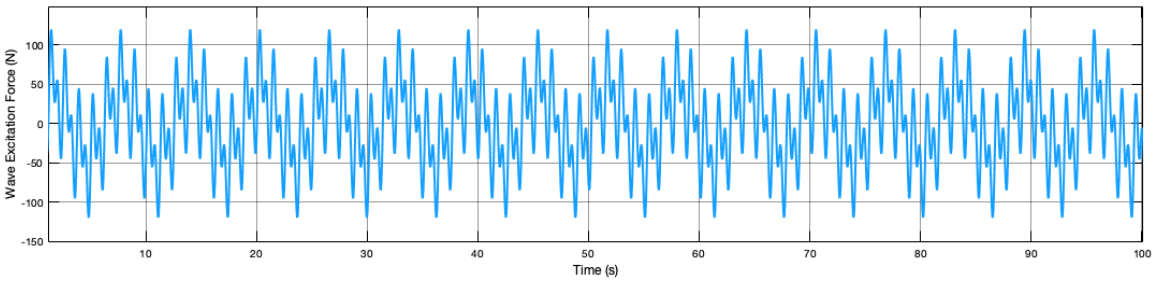

Figure 5.10: Wave Excitation Force

We can also notice in all the simulation result figures, the wave excitation force and moment (blue curve) have a high frequency as shown in Figure 5.10. The excitation force and moment used in WEC-Sim is nonlinear. Low damping of the system due to the lack of viscous damping is speculated to have caused the high frequency oscillations in the WEC system. These oscillations lead to cause high frequency excitation forces and moments, so for future studies the recommendation is to add viscous damping. The addition of damping to the system would help avoid instabilities in the system that cause high frequency oscillations.

Although this case study can be speculated to be promising based on the simulation results, it is important to note that the performance results are constrained by the 2 DOF robot design, the specific frequencies, the trial and error controller tuning method and the case study assumptions. In addition, the simulation study doesn't take into account other degrees-of-freedom in which forces are acting on the buoy. The elimination of high frequencies in wave excitation force and moment, optimizing controller parameters and other limitations are suggested for future work in the next chapter.

5.3 Conclusion

In this chapter, the wave energy converter case study results are provided. The chapter starts with an introduction to the WEC simulation software used to find the heave forces

and pitch moments acting on the buoy. The simulation results of the WEC control in the MATLAB-Simulink environment are also presented in this chapter. Performance of the proposed SM-ES controller was compared with the results of the latching controller. The results indicate the effectiveness of the proposed scheme in maximizing power absorption.

Chapter 6

Conclusion

6.1 Summary

In this thesis, a sliding-mode extremum seeking scheme is proposed, and its performance is studied through simulation studies in a near-shore (approximately 5 km off the coastline) wave energy converter control application. The key contributions of the present dissertation can be summarized as follows:

1. The objective was to extract maximum power from multi-frequency regular waves using a near-shore multi degrees-of-freedom serial chain WEC by controlling the speed of the system. Hence, a time-domain dynamic model for a generalized point absorber type WEC's is presented in this dissertation. The time-domain dynamic model can be used in future research and developments as a baseline model for robotic WEC's with power extraction in multiple degrees-of-freedom.
2. The controller design for maximum power absorption using the SM-ES scheme is presented. The dynamic time-domain model mentioned previously is used to find conditions for maximizing power transfer. These conditions are embedded into the SM-ES controller as a function of the WEC's velocity of motion.
3. Moreover, a simulated case study is performed on a custom 2 DOF wave energy conversion system. The velocity of the system is controlled using the proposed controller and the power absorption analyzed.
4. The simulation results demonstrate the efficiency of the proposed controller in achieving more average power absorption overtime (approximately 120 seconds) when compared with a latching controller. The proposed controller's average power output is 1.1 times the latching controller's output during heave motion after 120 seconds. Similarly, we can see that the average power output of the SM-ES controller is 1.5 times the latching controller during pitch motion after 115 seconds.

5. The results validate the effectiveness of the proposed controller in terms of power absorption for more than one DOF.

In the simulation case study, the proposed controller absorbs more average power in comparison to the latching controller. However, in the simulation results, we can observe that the wave excitation force and moment (blue curve) has a high frequency. There can be several reasons for this, perhaps a lack of viscous damping and simulation limitations with waveform generators. For future simulations, the recommendation is to include viscous damping.

Although, the simulation results indicate that this case study is likely to be promising. It is important to note that the performance results are limited by the 2 DOF robot design, the specific frequency, trial and error controller tuning, and the case study set-up. In addition, other degrees-of-freedom may be acting on the buoy, which are not taken into account in this simulation study. The waves used to simulate the dynamics of the WEC are also unrealistic as they are regular waves. Additionally, the elimination of high frequencies in wave excitation force and moment, optimizing controller parameters and other limitations are suggested for future work in the following section.

6.2 Suggestions for Future Research

This study is viable for future work in wave energy capture, robot impedance control [83], and many more. Future studies could also include adding the SM-ES controller to the WEC-Sim environment. A few suggestions are as follows:

6.2.1 Optimizing Control Parameter Tuning

The control parameters in this thesis were tuned using a trial and error method, and the WEC model is a dynamic simulation-based model. Therefore, in developing the control parameters presented here, the author had knowledge of the excitation force and moment values. These values are not accurately predetermined for a physical WEC in a wave tank or deployed at sea. However, the simulation-validated WEC model presented in this thesis can be used to gauge the performance of the control parameters in a physical WEC system. Another potential approach to improve control accuracy would be to have different control parameters for different sea states, and then switch between these configurations based on the present sea state characteristics.

6.2.2 Reactive Power Control

In this thesis, for achieving maximum power absorption, the velocity of the system was in-phase with the excitation force and moment. However, injecting reactive power to the

system might be beneficial during control instability. This work can be further developed to control the amount of active/reactive power injected to the feedback system.

6.2.3 Analyzing the Effect of Coupling Elements in the Proposed SM-ES Controller

In the proposed SM-ES controller, K is defined as an n $\times$ n diagonal positive definite matrix which determines the convergence rate. This leads to a straightforward stability analysis and low computational burden. If the coupling control parameters are considered as well, the precision of the control increases, which increases the system computational cost. This may not be suitable in some applications where fast tracking is required, thus a compromise is necessary. In this regard, studying the effect of coupling elements in the proposed SM-ES controller would be an interesting topic for future work.

Bibliography

[1] A. Kolios, L. F. D. Maio, L. Wang, L. Cui, and Q. Sheng. Reliability assessment of point-absorber wave energy converters. *Ocean Engineering*, 163:40 – 50, 2018.

[2] S. Chandrasekaran and H. Sinhmar. Power generation using mechanical wave energy converter. *The International Journal of Ocean and Climate Systems*, 3:57 – 70, 03 2012.

[3] S. Chandrasekaran and B. Raghavi. Design, development and experimentation of deep ocean wave energy converter system. *Energy Procedia*, 79:634 – 640, 2015.

[4] H.Y. Wang and Z.C. Sun. Experimental study of a porous floating breakwater. *Ocean Engineering*, 37(5):520 – 527, 2010.

[5] K. Hasselmann, W. Sell, D. B. Ross, and P. Müller. A parametric wave prediction model. *Journal of Physical Oceanography*, 6(2):200 – 228, 1976.

[6] M. P. Schoen, J. Hals, and T. Moan. Wave prediction and robust control of heaving wave energy devices for irregular waves. *IEEE Transactions on Energy Conversion*, 26(2):627 – 638, 2011.

[7] K. Osawa, H. Yamaguchi, M. Umair, M. A. Hashmani, and K. Horio. Wave height and peak wave period prediction using recurrent neural networks. *2020 International Conference on Computational Intelligence (ICCI)*, 11:1 – 4, 2020.

[8] G. Bacelli and R. G. Coe. Comments on control of wave energy converters. *IEEE Transactions on Control Systems Technology*, 29(1):478 – 481, 2021.

[9] D. Karmakar and C. G. Soares. Scattering of gravity waves by a moored finite floating elastic plate. *Applied Ocean Research*, 34:135 – 149, 2012.

[10] R. Pupadubsin, N. Chayopitak, D.G. Taylor, N. Nulek, S. Kachapornkul, P. Jitkreeyarn, P. Somsiri, and K. Tungpimolrut. Adaptive integral sliding-mode position control of a coupled-phase linear variable reluctance motor for high-precision applications. *IEEE Transactions on Industry Applications*, 48(4):1353 – 1363, 2012.

[11] M. K. Bugeja, S. G. Fabri, and L. Camilleri. Dual adaptive dynamic control of mobile robots using neural networks. *IEEE Transactions on Systems, Man, and Cybernetics, Part B (Cybernetics)*, 39(1):129 – 141, 2009.

[12] R. Wai and L. Chang. Adaptive stabilizing and tracking control for a nonlinear inverted-pendulum system via sliding-mode technique. *IEEE Transactions on Industrial Electronics*, 53(2):674 – 692, 2006.

[13] R. Genest and J. V. Ringwood. Receding horizon pseudospectral control for energy maximization with application to wave energy devices. *IEEE Transactions on Control Systems Technology*, 25(1):29–38, 2017.

[14] M. Guay and D. Dochain. A min max extremum-seeking controller design technique. *IEEE Transactions on Automatic Control*, 59(7):1874 – 1886, 2014.

[15] Z. O. Ilhan, Q. Wang, J. Barry, D. Huxley-Cohen, H. Wang, E. Schuster, S. Xie, M. Gilmore, and A. Ware. Extremum-seeking-based fluctuation mitigation and azimuthal velocity profile regulation by $e \times b$ actuation in helcat. *IEEE Transactions on Plasma Science*, 42(3):458 – 468, 2014.

[16] B. Hunnekens, A. D. Dino, N. Vd. Wouw, N. V. Dijk, and H. Nijmeijer. Extremum-seeking control for the adaptive design of variable gain controllers. *IEEE Transactions on Control Systems Technology*, 23(3):1041 – 1051, 2015.

[17] S. F. Toloue and M. Moallem. Multivariable sliding-mode extremum seeking control with application to mppt of an alternator-based energy conversion system. *IEEE Transactions on Industrial Electronics*, 64(8):6383 – 6391, 2017.

[18] P. Beirao and C.S.P. Malca. Design and analysis of buoy geometries for a wave energy converter. *International Journal of Energy Environmental Engineering*, 91, 2014.

[19] G. W. Boehlert and A. B. Gill. Environmental and ecological effects of ocean renewable energy development: A current synthesis. *Oceanography*, 23, June 2010.

[20] R. Bedard, P. T. Jacobson, M. Previsic, W. Musial, and R. Varley. An overview of ocean renewable energy technologies. *Oceanography*, 23, June 2010.

[21] J. Falnes. Optimum control of oscillation of wave-energy converters. *International Ocean and Polar Engineering Conference*, 12, June 2001.

[22] O. Kayode, O. Koya, and T. Ajewole. Determination of the optimal buoy shape for a concept wave energy converter to harness low amplitude sea waves using numerical simulation. *International Journal of Marine Engineering Innovation and Research*, 4, 2019.

[23] R. Song, M. Zhang, X. Qian, X. Wang, M. Dai, and J. Chen. A floating ocean energy conversion device and numerical study on buoy shape and performance. *Journal of Marine Science and Engineering*, 4:35, 05 2016.

[24] A. Saenz-Aguirre, A. Ulazia, G. Ibarra-Berastegui, and J. Saenz. Extension and improvement of synchronous linear generator based point absorber operation in high wave excitation scenarios. *Ocean Engineering*, 239:109844, 2021.

[25] H. R. Ghafari, H. Ghassemi, and G. He. Numerical study of the wavestar wave energy converter with multi-point-absorber around deepcwind semisubmersible floating platform. *Ocean Engineering*, 232:109177, 2021.

[26] D. García-Violini, Y. Peña-Sanchez, N. Faedo, C. Windt, F. Ferri, and J. V. Ringwood. Experimental implementation and validation of a broadband lti energy-maximizing control strategy for the wavestar device. *IEEE Transactions on Control Systems Technology*, 29(6):2609 – 2621, 2021.

[27] P. Hart and R. Lurie. Application of powerbuoy wave energy converter technology to remote power requirements in oil and gas field developments. *OTC Offshore Technology Conference*, 3, 04 2012.

[28] T. Pan, Z. Ji, and Z. Jiang. Maximum power point tracking of wind energy conversion systems based on sliding mode extremum seeking control. *2008 IEEE Energy 2030 Conference*, 8:1 – 5, 2008.

[29] E. Baker, S. Evans, J. Foster-Smith, A. Incecik, and A. Mesbahi. Marine science and technology for environmental sustainability. *3rd International Conference ENSUS*, 27, 2005.

[30] M. Ravindran and P. M. Koola. Energy from sea waves—the indian wave energy program. *Current Science*, 60(12):676 – 680, 1991.

[31] F. Wahid, T. Sanjana, A. Roy, Q. Tareq, and M. A. Karim. Designing of a pelamis wave energy converter in matlab simulink and studying the output characteristics with variation to electrical and mechanical parameters. *2017 4th International Conference on Advances in Electrical Engineering (ICAEE)*, 9:669 – 674, 2017.

[32] Z. Zhou, W. Knapp, J. MacEnri, H. Ch. Sorensen, E. F. Madsen, I. Masters, and P. Igic. Permanent magnet generator control and electrical system configuration for wave dragon mw wave energy take-off system. *2008 IEEE International Symposium on Industrial Electronics*, 7:1580 – 1585, 2008.

[33] C. Windt, N. Faedo, M. Penalba, and J. V. Ringwood. Assessment of the evaluation framework for energy maximizing control systems for the wavestar wave energy converter. *2019 American Control Conference (ACC)*, 9:4791 – 4796, 2019.

[34] O. Farrok, K. Ahmed, A. D. Tahlil, M. Farah, M. Kiran, and Md. R. Islam. Electrical power generation from the oceanic wave for sustainable advancement in renewable energy technologies. *Sustainability*, 12:1 – 23, 03 2020.

[35] A. Ghasemi. Computational simulation of the interaction between moving rigid bodies and two-fluid flows. *Computers and Fluids*, 09 2013.

[36] R. Vertechy, M. Fontan, G. Rosati, and M. Bergamasco. Oscillating-water-column wave-energy-converter based on dielectric elastomer generator. *The International Society for Optical Engineering*, 8687:86870I, 04 2013.

[37] S. Ortega-Achury, W. Mcanally, T. Davis, and J. Martin. Hydrokinetic power review. *Mississippi State University Report*, 06 2022.

[38] D. O'Sullivan, D. Mollaghan, A. Blavette, and R. Alcorn. Dynamic characteristics of wave and tidal energy converters and a recommended structure for development of a generic model for grid connection. *Integration of Ocean Energy Plants into Distribution and Transmission Electrical Grids*, 01 2010.

[39] M. Hall, B. Buckham, C. Crawford, and R. S. Nicoll. The importance of mooring line model fidelity in floating wind turbine simulations. *Oceans IEEE Conference*, 11:1 – 8, 2011.

[40] K. Ruehl, D. Ogden, Y. Yu, A. Keester, N. Tom, D. Forbush, and J. Leon. Review of wec-sim development and applications. *in Proceedings of the 14th European Wave and Tidal Energy Conference*, EWTEC 2021.

[41] K. Ruehl, D. Ogden, Y. Yu, A. Keester, N. Tom, D. Forbush, J. Leon, J. Grasberger, and S. Husain. Wec-sim v5.0.1. *WEC-Sim Documentation*, 2022.

[42] M. Faizal, M. R. Ahmed, and Y-H. Lee. A design outline for floating point absorber wave energy converters. *Advances in Mechanical Engineering*, 6, 2014.

[43] G. S. Payne, J. R. M. Taylor, T. Bruce, and P. Parkin. Assessment of boundary-element method for modelling a free-floating sloped wave energy device. part 1: Numerical modelling. *Ocean Engineering*, 35:333 – 341, 2008.

[44] R. Coe, G. Bacelli, and D. Forbush. A practical approach to wave energy modeling and control. *Renewable and Sustainable Energy Reviews*, 142:110791, 05 2021.

[45] M. R. Dhanak and N. I. Xiros. Springer handbook of ocean engineering. *Springer-Verlag GmbH Berlin Heidelberg*, 2016.

[46] E. A. Shami, R. Zhang, and X. Wang. Point absorber wave energy harvesters: A review of recent developments. *Energies*, 12, 2019.

[47] S. Zou, O. Abdelkhalik, R. Robinett, G. Bacelli, and D. Wilson. Optimal control of wave energy converters. *Renewable Energy*, 103, 2016.

[48] Y. Vora. Dynamic simulation of robot manipulators. *Oregon State University*, 1985.

[49] R. Tedrake. Robot manipulation: Perception, planning, and control. *Course Notes for MIT 6.881*, 2020.

[50] K. Budal and J. Falnes. Optimum operation of wave power converter. *Marine Science Community United States*, 1976.

[51] J. Falnes and P. M. Lillebekken. Budal's latching-controlled-buoy type wave-power plant. *5th European Wave Energy Conference*, 2003.

[52] J. Falnes and T. Bjarte-Larsson. Theoretical and experimental investigation of wave energy conversion by a phase-controlled heaving body. *Journal of Engineering for the Maritime Environment*, 220:175 – 183, 2006.

[53] M. Jama, B. F. Mon, A. Wahyudie, and S. Mekhilef. Maximum energy capturing approach for heaving wave energy converters using an estimator-based finite control set model predictive control. *IEEE Access*, 9:67648 – 67659, 2021.

[54] A. Maria-Arenas, A. J. Garrido, E. Rusu, and I. Garrido. Control strategies applied to wave energy converters: State of the art. *Energies*, 12(16):3115, Aug 2019.

[55] Y. Zhang and G. Li. Non-causal linear optimal control of wave energy converters with enhanced robustness by sliding mode control. *IEEE Transactions on Sustainable Energy*, 11(4):2201 – 2209, 2020.

[56] N. Faedo, Y. Peña-Sanchez, and J. V. Ringwood. Receding-horizon energy-maximising optimal control of wave energy systems based on moments. *IEEE Transactions on Sustainable Energy*, 12(1):378 – 386, 2021.

[57] N. Faedo, G. Scarciotti, A. Astolfi, and J. V. Ringwood. Nonlinear energy-maximizing optimal control of wave energy systems: A moment-based approach. *IEEE Transactions on Control Systems Technology*, 29(6):2533 – 2547, 2021.

[58] M. S. Aftab and A. Wahyudie. Control force limitation in wave energy converter using neuro-adaptive hierarchical control scheme. *2018 5th International Conference on Renewable Energy: Generation and Applications (ICREGA)*, 5:132 – 135, 2018.

[59] Y. Pan. Extremum seeking control with sliding mode. *IFAC Proceedings Volumes*, 35(1):371–376, 2002.

[60] S. H. Kamali, M. Moallem, and S. Arzanpour. A two-variable extremum seeking controller with application to self-tuned vibration energy harvesting. *Smart Materials and Structures*, 28, 01 2019.

[61] A. Babarit and A.H. Clément. Optimal latching control of a wave energy device in regular and irregular waves. *Applied Ocean Research*, 28(2):77 – 91, 2006.

[62] P. Borne, G. Dauphin-Tanguy, J.P. Richard, F. Rotella, and I. Zambettakis. Méthodes et techniques de l'ingénieur, automatique: Commande et optimisation des processus. *TECNIP-Paris*, 1990.

[63] H. Cho and S. Yu. Performance evaluation of a long-range marine communication system for fishing buoy detection. *2019 IEEE Underwater Technology (UT)*, 4:1 – 5, 2019.

[64] S. Baba, Y. Ota, T. Fukuda, Y. Ishihara, T. Murashima, and Y. Amitani. Development of an oceanographic observation buoy for rough and icy sea conditions. *Oceans'11 MTS/IEEE Kona*, 5:1 – 5, 2011.

[65] H. Ochi, Y. Ishihara, and T. Sugiyama. Concept of a tsunami warning buoy system and an acoustic telemetry system for high current area. *2012 Oceans at Yeosu*, 3:1 – 3, 2012.

[66] T. A. Vandall. Advances in buoy technology for navigation, meteorology and oceanography. 2:1109 – 1114, 2000.

[67] S. G. P. Skey and M. D. Miles. Advances in buoy technology for wind/wave data collection and analysis. *Oceans '99. MTS/IEEE. Riding the Crest into the 21st Century. Conference and Exhibition. Conference Proceedings (IEEE Cat. No.99CH37008)*, 1:113 – 118, 1999.

[68] M. Folley and T. Whittaker. Analysis of the nearshore wave energy resource. *Renewable Energy*, 34:1709 – 1715, 07 2009.

[69] A. Cornett and J. Zhang. Nearshore wave energy resources, western vancouver island, b.c. *Canadian Hydraulics Center National Research Council of Canada*, Technical Report, April 2008.

[70] A. Cornett. A global wave energy resource assessment. *Conference Paper in Sea Technology*, 2008.

[71] J. Goggins and W. Finnegan. Shape optimization of floating wave energy converters for a specified wave energy spectrum. *Renewable Energy*, 71:208 – 220, 2014.

[72] L. Bruzzone, P. Fanghella, and G. Berselli. Reinforcement learning control of an onshore oscillating arm wave energy converter. *Ocean Engineering*, 206:107346, 2020.

[73] R. Jha. Wave measurement methodology and validation from wave glider unmanned surface vehicles. *2018 OCEANS - MTS/IEEE Kobe Techno-Oceans (OTO)*, 6:1 – 7, 2018.

[74] H. Roh, H. Joe, S. Seokyong, M. Sung, and S. Yu. Hydrodynamic modeling and optimization of mobile wave energy harvesting system for the robotic buoy. *OCEANS 2016 MTS/IEEE Monterey*, 4:1 – 4, 2016.

[75] W. Zhu, X. Wang, M. Xu, J. Yang, T. Si, and S. Zhang. A wave energy conversion mechanism applied in robotic fish. *2013 IEEE/ASME International Conference on Advanced Intelligent Mechatronics*, 3:319 – 324, 2013.

[76] H. Joe, M. Kim, S. Wi, H. Kwon, and S. Yu. Development of mooring-less robotic buoy system using wave powered renewable energy. *2014 Oceans at St. John's*, 2:1 – 6, 2014.

[77] R. Murray, Z. Li, and S. Sastry. A mathematical introduction to robot manipulation. *CRC Press, Boca Raton*, 29, 12 2010.

[78] A. Maravandi. Directed studies ii report: Design of robotic arm for wave energy conversion. *Unpublished Manuscript*, 2010.

[79] J.J. Craig. Introduction to robotics. *Addison-Wesley Pub. Co.*, 2005.

[80] R. So, B. Bosma, K. Ruehl, and T. K. A. Brekken. Modeling of a wave energy oscillating water column as a point absorber using wec-sim. *IEEE Transactions on Sustainable Energy*, 11(2):851 – 858, 2020.

[81] R. So, C. Michelen, B. Bosma, P. Lenee-Bluhm, and T. K. A. Brekken. Statistical analysis of a 1:7 scale field test wave energy converter using wec-sim. *IEEE Transactions on Sustainable Energy*, 8(3):1118 – 1126, 2017.

[82] K. Ruehl, C. M. Ströfer, S. Kanner, M. Lawson, and Y. Yu. Preliminary verification and validation of wec-sim, an open-source wave energy converter design tool. *International Conference on Offshore Mechanics and Arctic Engineering (OMAE)*, 9:40, 06 2014.

[83] G. A. Folkertsma and S. Stramigioli. Energy in robotics. *Foundations and Trends in Robotics*, 6(3):140 – 210, 2017.

Appendix A

Supplementary Images

In this section, the following Figures are provided for reference.

Figure A.1 represents dimensions of the buoy measured in SolidWorks.

Figure A.2 is a block diagram depicting the workflow of the Proposed Sliding Mode Extremum Seeking (SM-ES) Controller with Maximum Power Transfer Function.

Figure A.3 is a block diagram depicting the workflow of the Wave Energy Converter Simulator (WEC-Sim) modeling process.

Figure A.4 is the simulation results until average power reaches steady state, when a latching controller is applied to the Wave Energy Converter (WEC) system in heave motion.

Figure A.5 is the simulation results until average power reaches steady state, when a latching controller is applied to the WEC system in pitch motion.

Figure A.6 is the simulation results until average power reaches steady state, when the Proposed SM-ES Control is applied to the WEC system in heave motion.

Figure A.7 is the simulation results until average power reaches steady state, when the Proposed SM-ES Control is applied to the WEC system in pitch motion.

Figures A.8 - A.12 represent the front, top, side and back view of the WEC assembly.

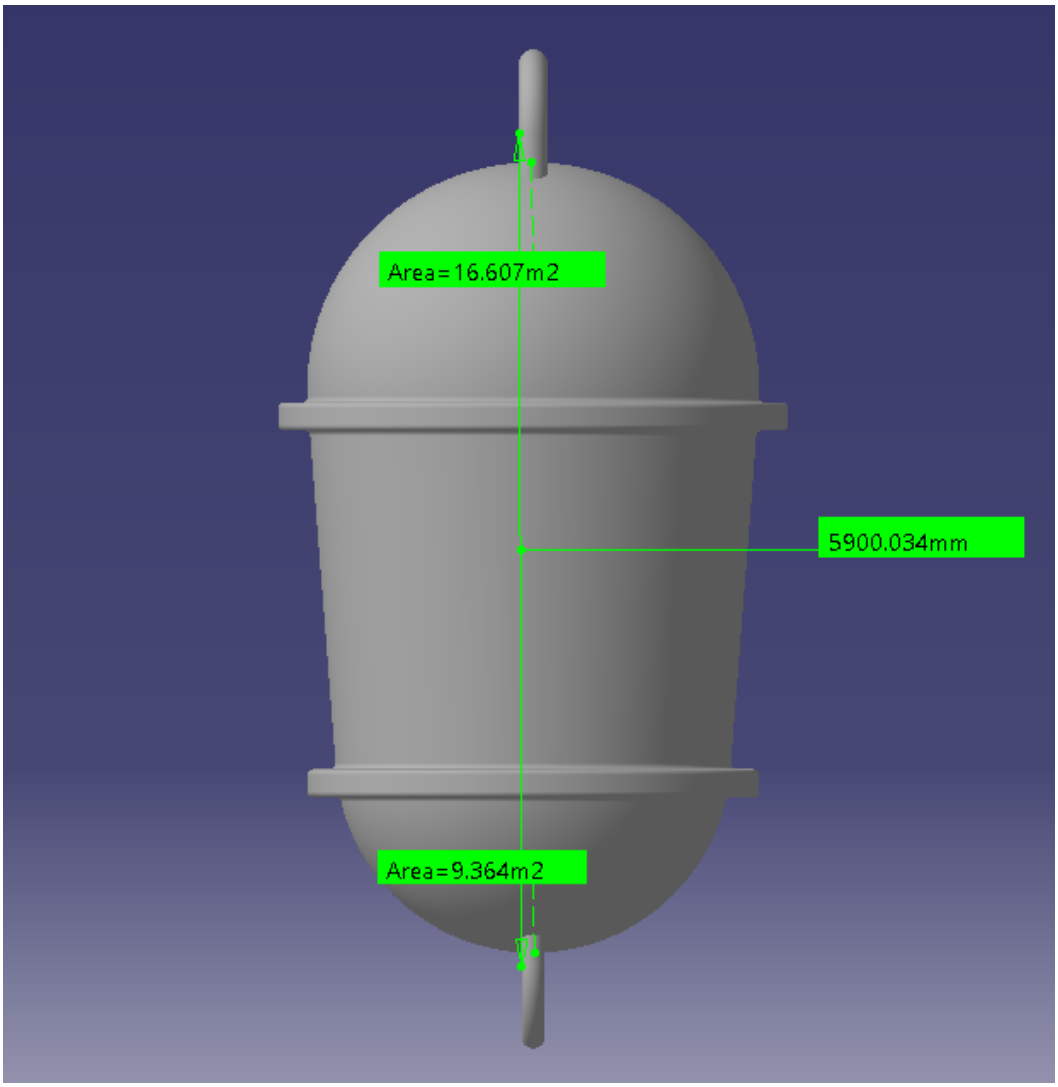

Figure A.1: Buoy Dimensions

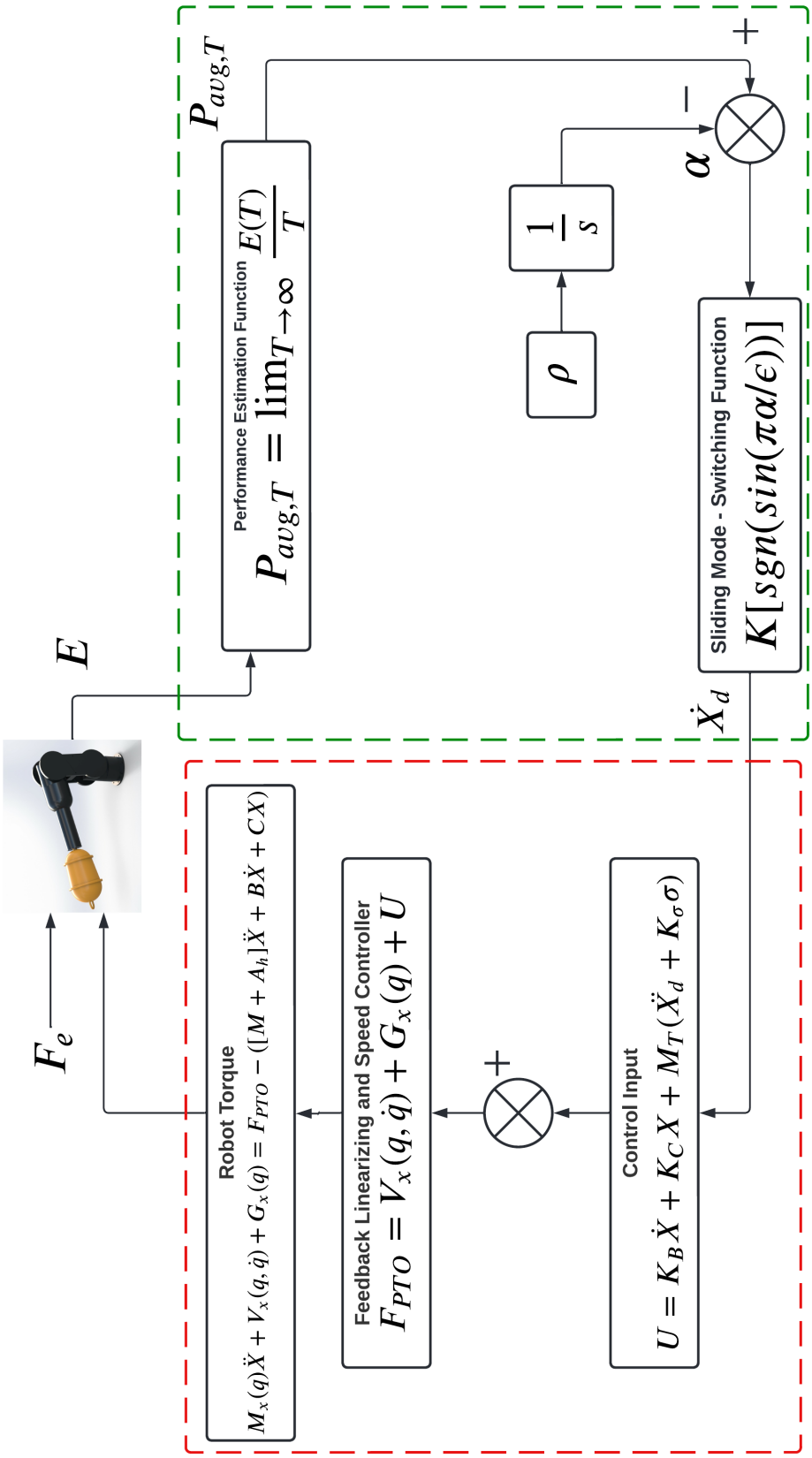

Figure A.2: Workflow of the Proposed SM-ES Controller with Maximum Power Transfer Function (P in this figure represents Power)

Figure A.3: WEC-Sim modeling Process

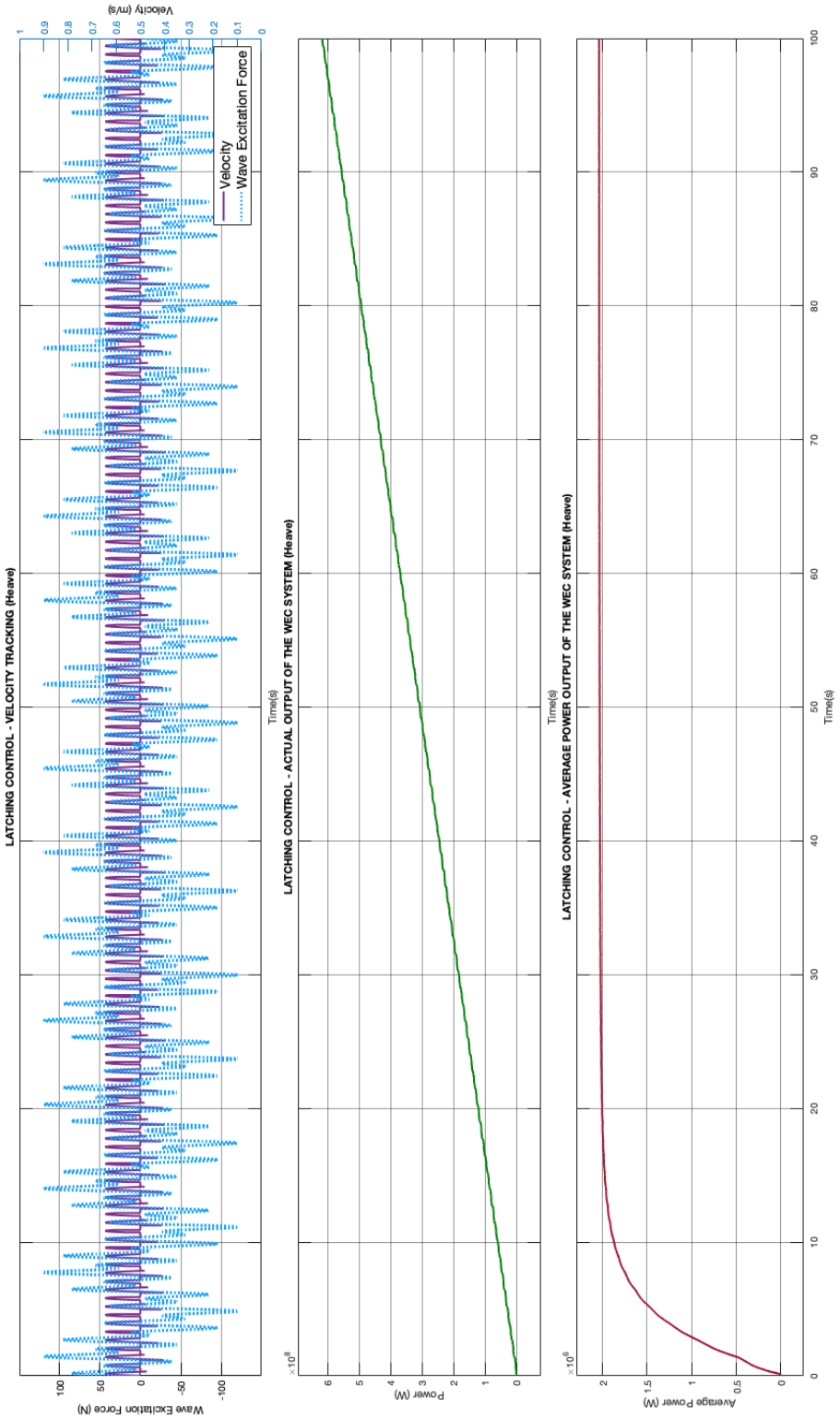

Figure A.4: Simulation results when a latching controller is applied to the WEC system – Heave motion

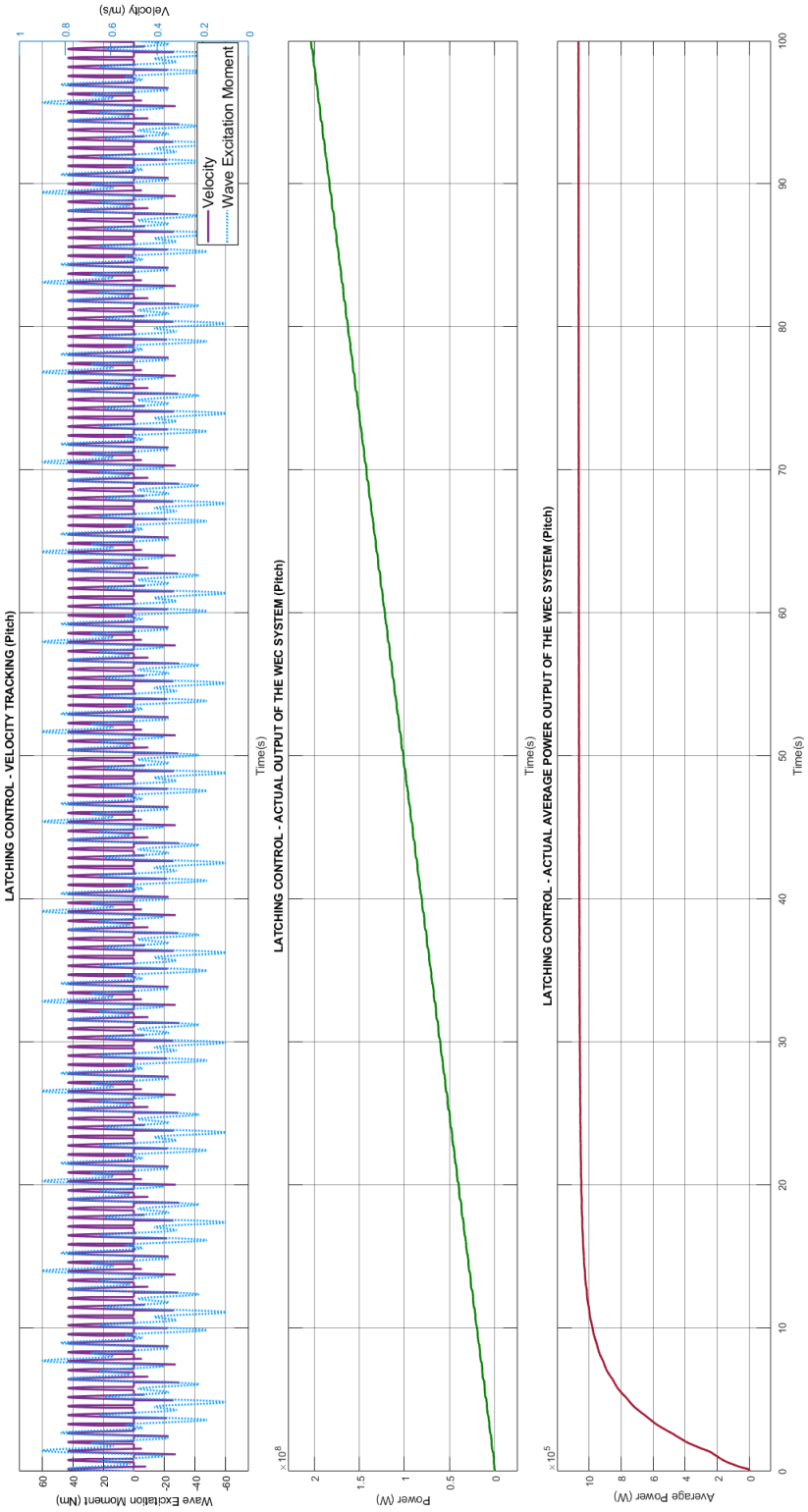

Figure A.5: Simulation results when a latching controller is applied to the WEC system – Pitch motion

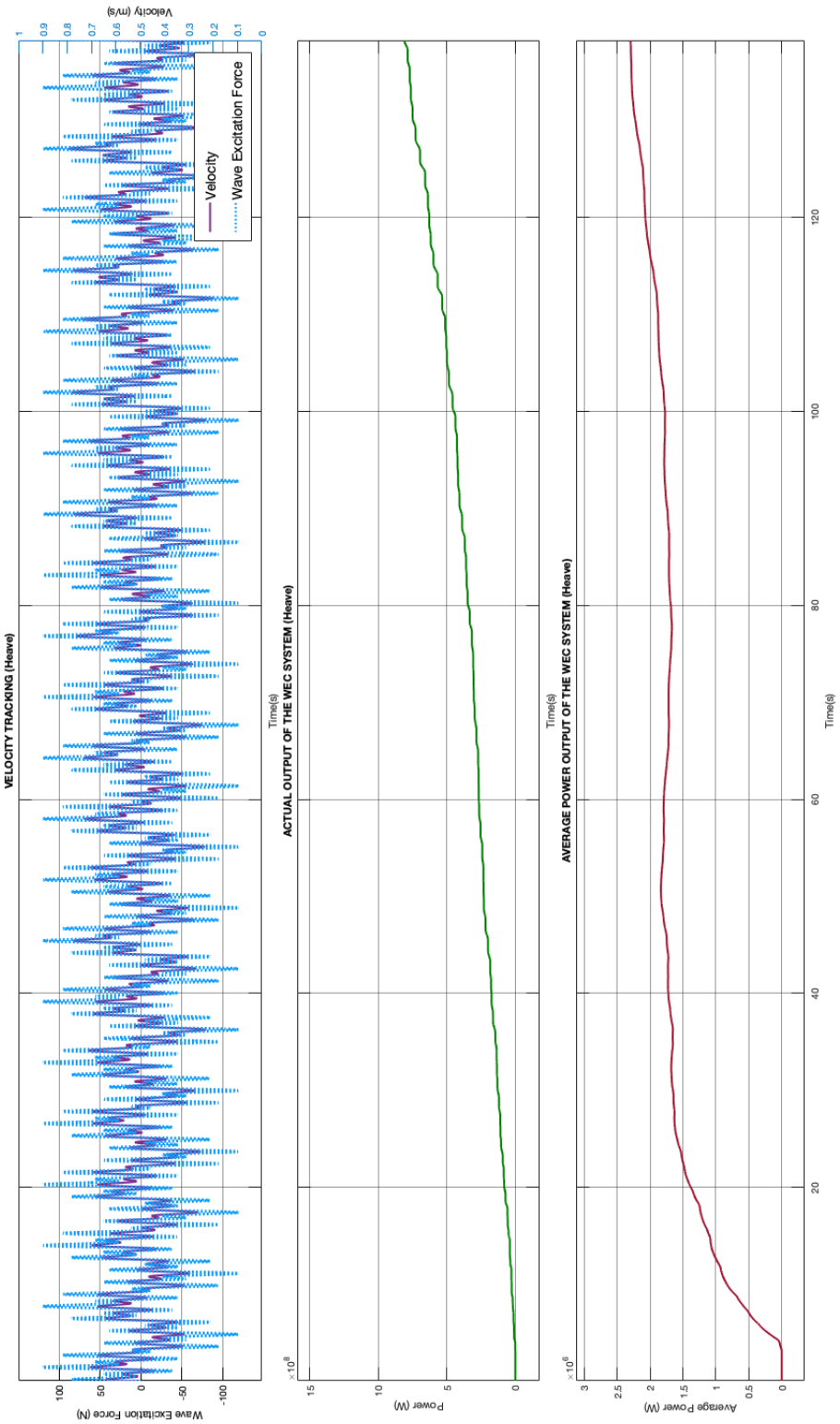

Figure A.6: Simulation results when the proposed SM-ES controller is applied to the WEC system – Heave motion

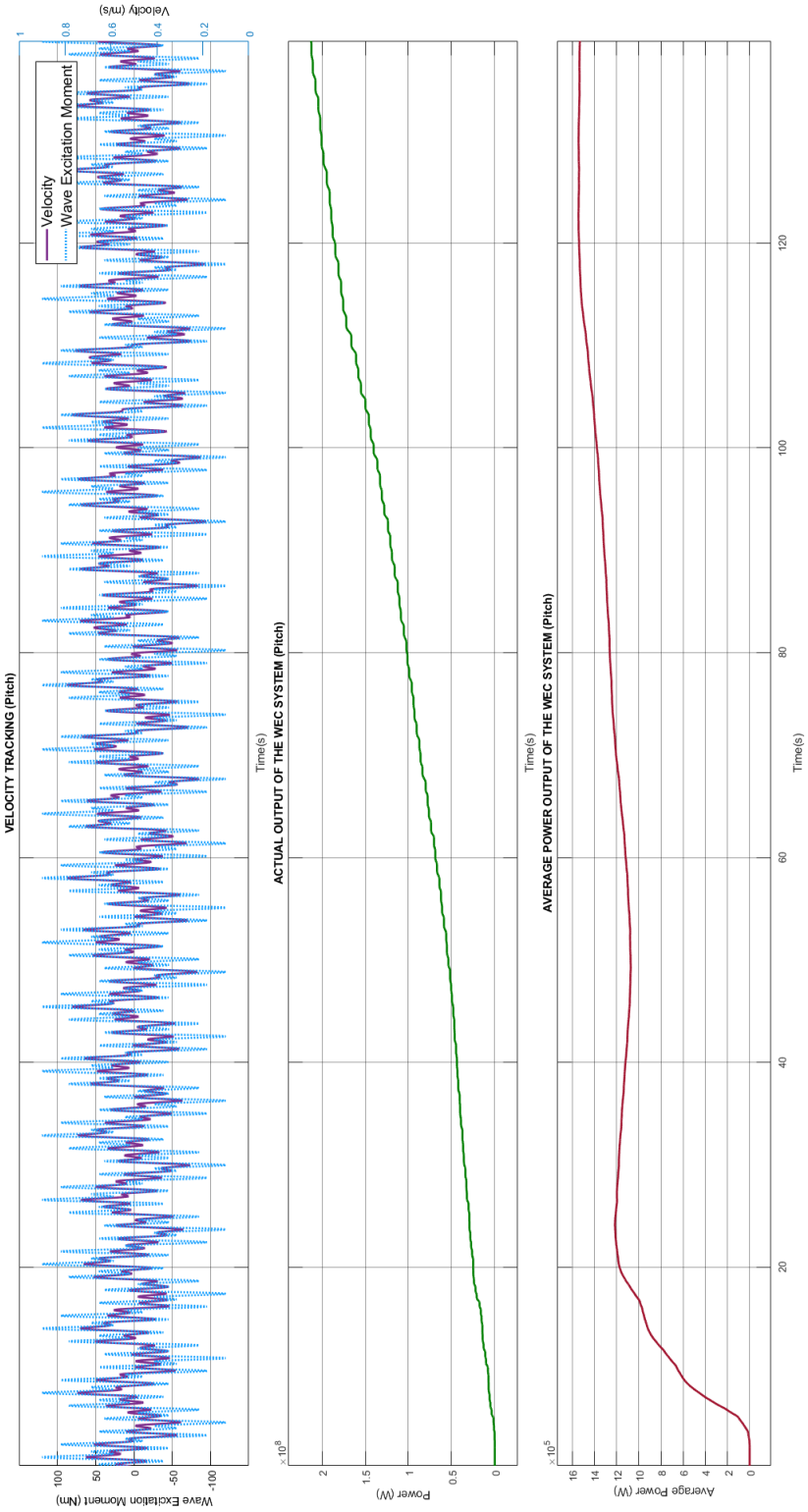

Figure A.7: Simulation results when the proposed SM-ES controller is applied to the WEC system – Pitch motion

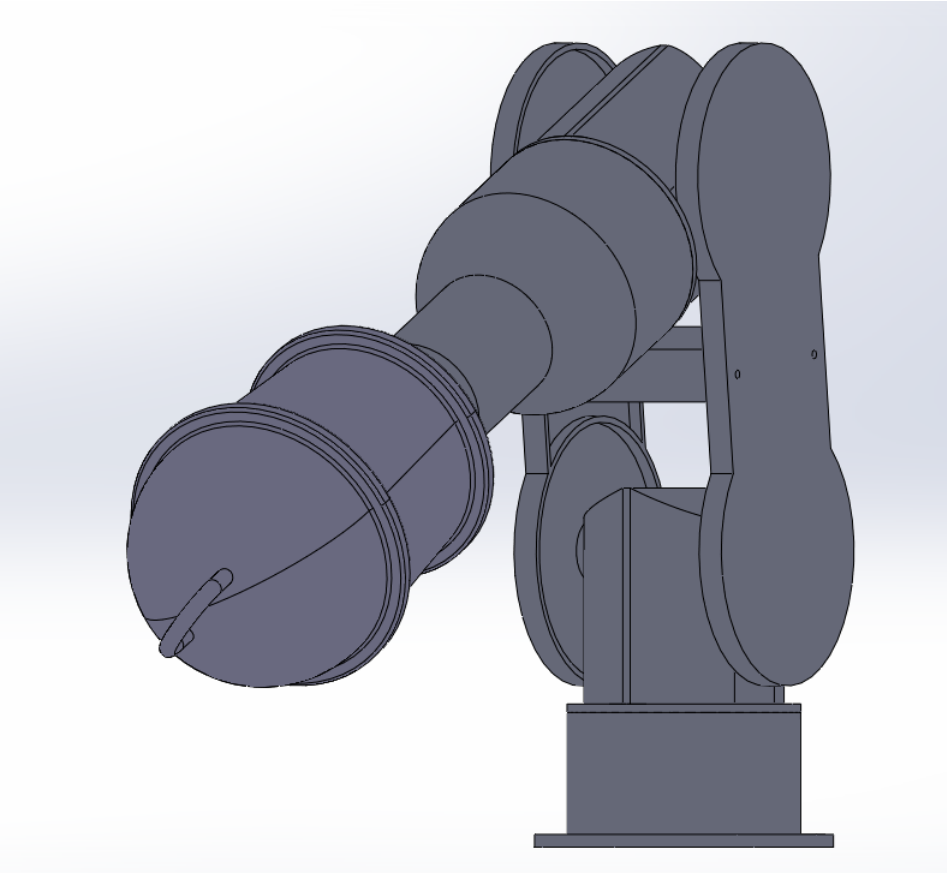

Figure A.8: WEC Assembly - Front View

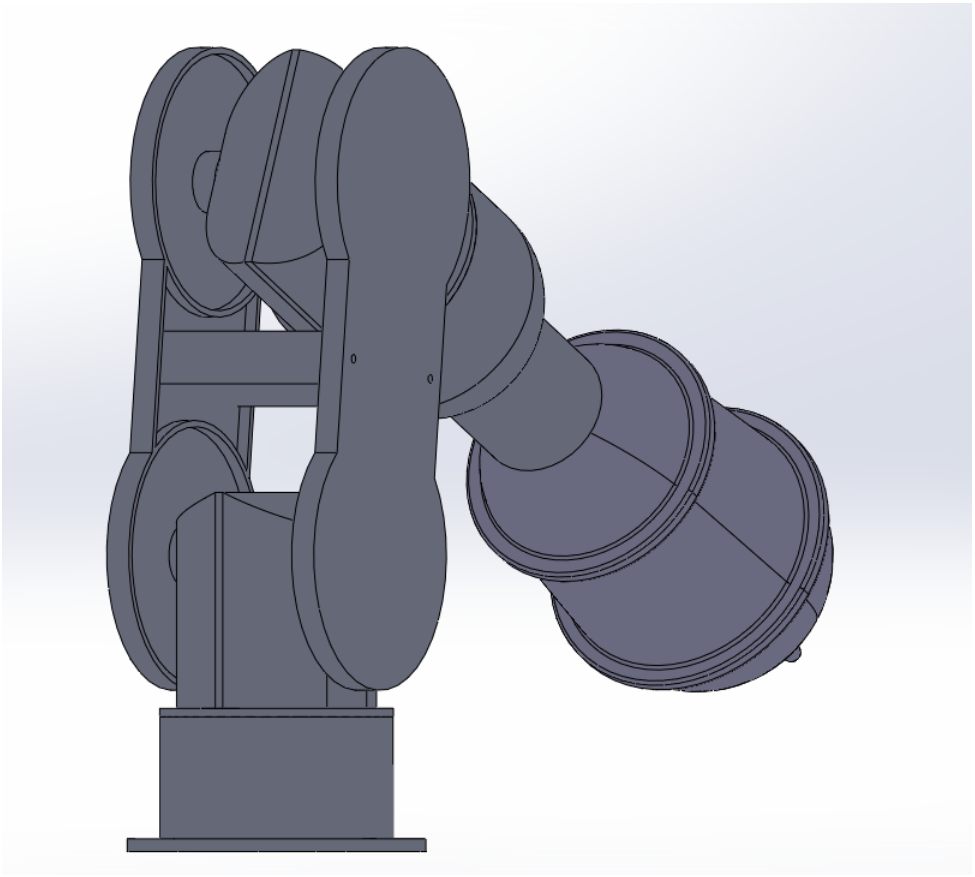

Figure A.9: WEC Assembly - Back View

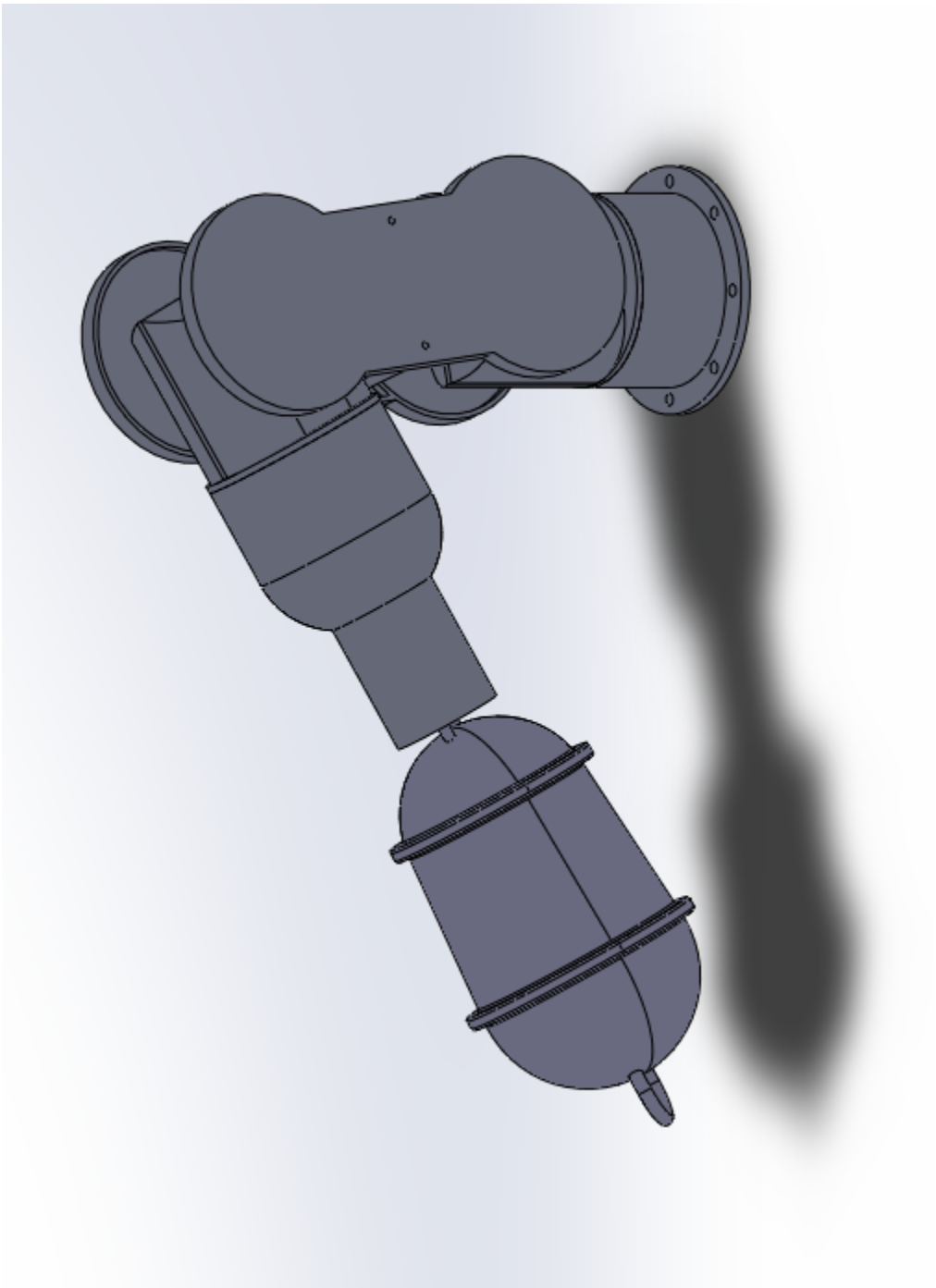

Figure A.10: WEC Assembly - Top View

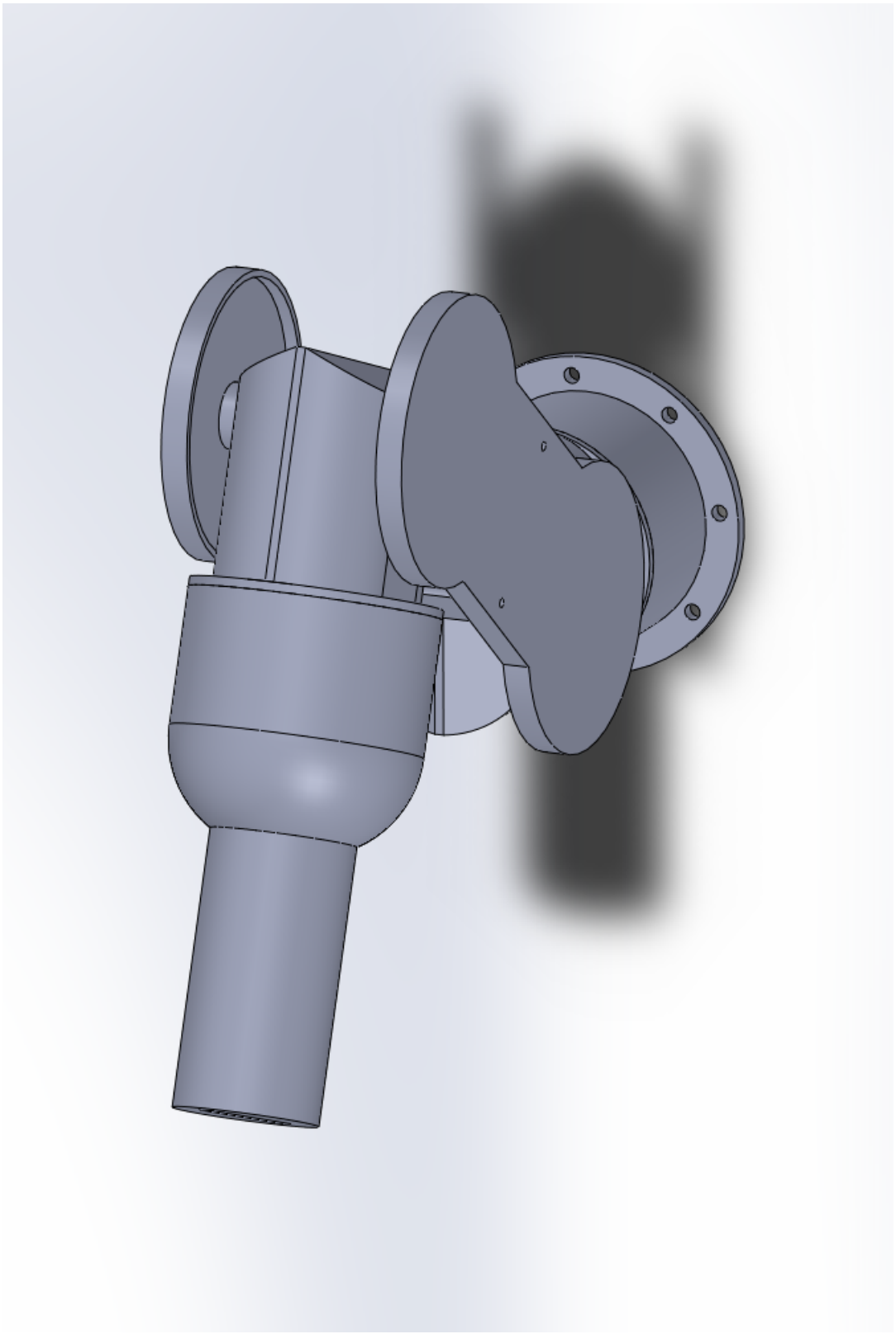

Figure A.11: WEC Assembly without Buoy - Side View

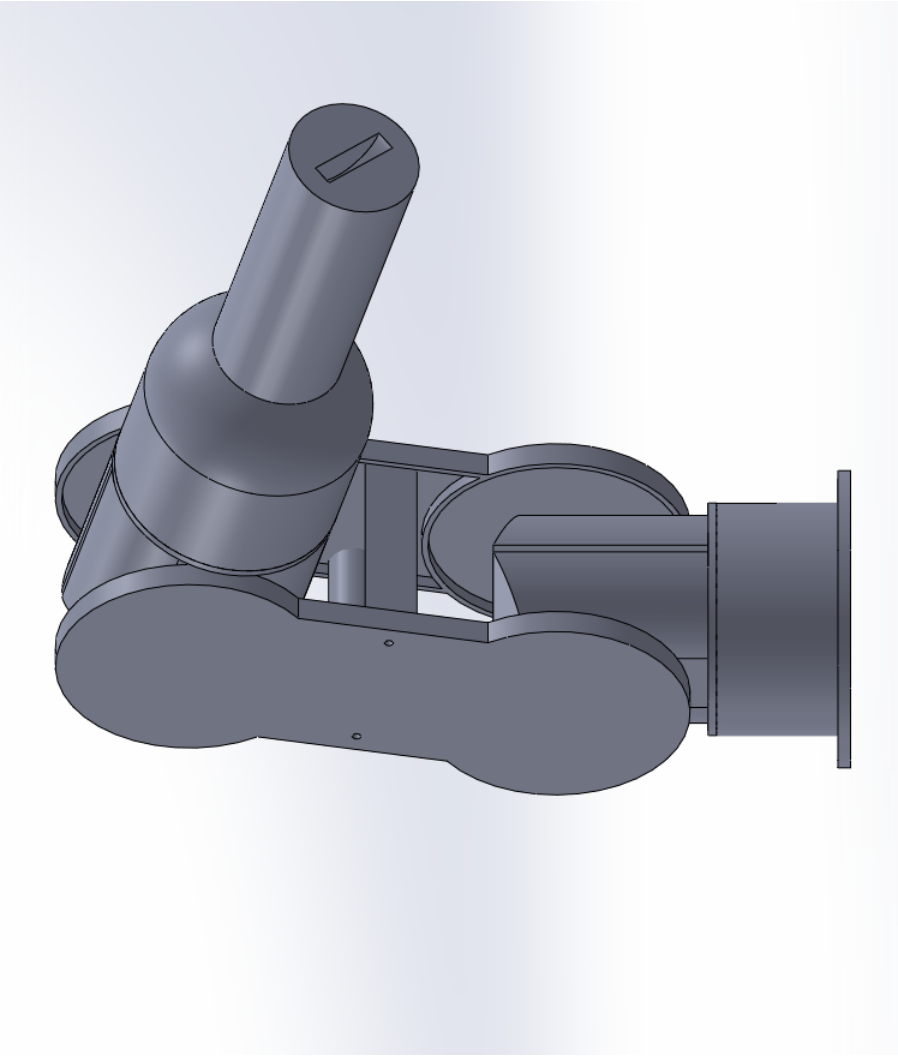

Figure A.12: WEC Assembly without Buoy - Side View